PHILOSOPHICAL TRANSACTIONS OF THE ROYAL SOCIETY A MATHEMATICAL, PHYSICAL & ENGINEERING SCIENCES

Interactions of polarized electrons and polarized photons with atoms and molecules

The Royal Society

Phil. Trans. R. Soc. Lond. A 1999 **357**, 1229-1258
doi: 10.1098/rsta.1999.0372

THE ROYAL SOCIETY

Interactions of polarized electrons and polarized photons with atoms and molecules

By Hans Kleinpoppen[1] and Uwe Becker[2]

[1]*Atomic Physics Laboratory, University of Stirling, Stirling FK9 4LA, UK*

[2]*Fritz-Haber-Institut der Max-Planck-Gesellschaft, Faradayweg 4-6, D-14195 Berlin, Germany*

In this paper, we initially list 23 subfields of the research topics associated with the title of this paper. Then we present a detailed theoretical description of polarized-electron interactions with atoms and molecules. Spin effects based on Coulomb-direct, Coulomb-exchange and spin–orbit interactions in light and heavy atoms are described, and experimental data are presented as tests for relevant theoretical approximations.

Electron-scattering interactions with orientated molecules such as CH_3I and CH_3Cl show interesting alignment and orientation effects, which are new types of test quantities for the theory of such electron-scattering processes with molecules.

Numerous multielectron effects determine photoionization of atoms in general. Spin, and spin–orbit interaction effects particularly, can be studied by photoelectron spin experiments and by applying polarized atoms in the photoionization process. The former type of experiment has been used very successfully in the photoionization of rare gas atoms, while the latter type of experiment and related theories have been applied particularly for photoionization with partly filled subshells. Out of such photoionization experiments with polarized atoms we selected one involving oxygen atoms $\{O(1s^2 2s^2 2p^4)\,^3P_2 + h\nu\}$ for a more detailed description.

While the photoionization process with unpolarized oxygen atoms is characterized by the cross-section, σ, and the angular distribution parameter, β, only; a further parameter, β', is required for photoionization with polarized oxygen atoms. Alternatively, it is possible to describe the photoionization of polarized oxygen atoms by deriving β and β' from the ratio of two reduced matrix elements for s and d electrons and their relative phase difference.

Keywords: polarized-electron and polarized-atom interactions; scattering of electrons by orientated molecules; photoionization of polarized atoms; 'complete' scattering experiments

1. Introductory remarks

As with most modern research areas, the subfields connected with the title of this paper have been developed to a high degree both in quality and quantity.

Therefore, in this article we can only highlight a few of the recent outstanding achievements in this active area of research. Nonetheless, we should, for completeness, briefly list the various successful subfields of research in the field of electron–atom and molecular collisions and photon interactions with atoms in which spin-dependent processes have been studied.

(1) Polarization in multiphoton ionization of atoms in intense laser fields.

(2) Atomic interaction with polarized particles and fields.

(3) Polarization effects in inner-shell excitation.

(4) Collisions of cooled and polarized sodium atoms.

(5) Spin polarization and rotation in photoionization.

(6) Sources and detectors of polarized electrons.

(7) Polarization, correlation and coherence lengths of two-photon radiation.

(8) Photoionization and fluorescence of atoms in giant resonance regions.

(9) Spin-polarized-electron scattering in condensed matter: an atomic approach.

(10) Circular dichroism in double-photoionization of atoms studied by electron time-of-flight coincidence spectroscopy.

(11) New physics in spin-dependent (e, 2e) collisions.

(12) Laser-assisted and laser-produced scattering.

(13) Resonance effects in multiphoton ionization.

(14) Scattering of polarized electrons from atoms and molecules.

(15) Chiral effects in electron scattering by molecules.

(16) (e, eγ) and (e, 2e) experiments involving polarized electrons.

(17) The stepwise excitation electron–photon coincidence technique.

(18) The photon–photon correlation experiments.

(19) Spin polarization of Auger electrons.

(20) Electron optic dichroism.

(21) Spin asymmetries in relativistic (e, 2e) processes.

(22) Photoionization of polarized atoms: applications to free atoms and ferromagnets.

(23) Two-photon polarization Fourier spectroscopy of atoms.

PHILOSOPHICAL TRANSACTIONS OF THE ROYAL SOCIETY A MATHEMATICAL, PHYSICAL & ENGINEERING SCIENCES

Table 1.

scattering process	amplitudes	cross-sections	
$\mathrm{e}(\uparrow) + \mathrm{a}(\downarrow) \rightarrow \mathrm{a}(\downarrow) + \mathrm{e}(\uparrow)$	f	$\lvert f\rvert^2$	reaction (1)
$\rightarrow \mathrm{a}(\uparrow) + \mathrm{e}(\downarrow)$	g	$\lvert g\rvert^2$	reaction (2)
$\mathrm{e}(\uparrow) + \mathrm{a}(\uparrow) \rightarrow \mathrm{a}(\uparrow) + \mathrm{e}(\uparrow)$	$f - g$	$\lvert f - g\rvert^2$	reaction (3)

2. Interactions of polarized electrons with atoms

In general, the directions of spins of colliding electrons, ions and atoms are randomly distributed. However, the spins of these particles can be polarized and an analysis of spin effects after the collision can provide new information on the dynamics of the collisional interaction, information that cannot be obtained by any other collision technique. Investigations of such spin effects require complicated instrumentation, which we will mention only briefly.

As usual, we define the degree of polarization of electrons and atoms as

$$P_\mathrm{e} = \frac{N_\mathrm{e}(1/2) - N_\mathrm{e}(-1/2)}{N_\mathrm{e}(1/2) + N_\mathrm{e}(-1/2)}, \qquad P_\mathrm{a} = \frac{N_\mathrm{a}(1/2) - N_\mathrm{a}(-1/2)}{N_\mathrm{a}(1/2) + N_\mathrm{a}(-1/2)},$$

where $N_\mathrm{e} = N_\mathrm{e}(1/2) + N_\mathrm{e}(-1/2)$ and $N_\mathrm{a} = N_\mathrm{a}(1/2) + N_\mathrm{a}(-1/2)$ are the total numbers of electrons and atoms with spins parallel $(+1/2)$ or antiparallel $(-1/2)$ to a given quantization direction.

The quantum mechanical expectation value for the spin polarization $\langle\sigma\rangle$, which is identical to the above macroscopic polarization, follows from Schrödinger's equation with Pauli's spin eigenfunction ψ as $\langle\sigma\rangle = \langle\psi \mid \sigma \mid \psi\rangle = P$. The polarization $\boldsymbol{P}$ is a vector quantity, i.e.

$$|\boldsymbol{P}| = \sqrt{|P_x|^2 + |P_y|^2 + |P_z|^2},$$

in which the above macroscopic definition is applied to each Cartesian coordinate.

Experiments with polarized electrons and polarized atoms carried out so far can be classified as follows:

(1) scattering of partly polarized electrons by partly polarized single-electron atoms (H, Li, Na, etc.);

(2) Mott scattering of unpolarized electrons by heavy polarized atoms; and

(3) scattering of unpolarized electrons by partly polarized atoms associated with polarization measurements of the outgoing electrons or the recoiling atoms.

In order to understand such experiments, we first develop a set of scattering amplitudes and apply them to the first case (Kleinpoppen 1971). We will assume that the electrons and the atoms are completely polarized, i.e. $|\boldsymbol{P}_\mathrm{e}| = 1$ and $|\boldsymbol{P}_\mathrm{a}| = 1$. We then distinguish the following 'spin reactions' between electrons completely polarized parallel or antiparallel to a given axis of quantization and characterized by the notations $\mathrm{e}(\uparrow)$ and $\mathrm{e}(\downarrow)$ for electrons on the one hand, and for polarized atoms with analogous notations $\mathrm{a}(\uparrow)$ and $\mathrm{a}(\downarrow)$ on the other hand (see table 1).

In the first reaction, a *direct Coulomb interaction* takes place, in which the spin directions of both particles are conserved since the projectile electron is not

exchanged with the atomic electron. We associate a *direct scattering amplitude* f and its differential cross-section $\sigma_{\rm d} = |f|^2$ with this collisional interaction. In the second reaction, an *electron exchange* between the incoming electron and the atomic electron takes place; the amplitude associated with this interaction is the *exchange amplitude* g and its differential exchange cross-section is $\sigma_{\rm ex} = |g|^2$. The third reaction is described by a *coherent superposition* or *interference* between the direct Coulomb and exchange interactions, both of which take place in the collision but cannot be separated from each other contrary to the first two reactions; the resulting amplitude describing the third process is an *interference amplitude* $f - g$, and its differential cross-section $\sigma_{\rm int} = |f - g|^2$. The minus sign between f and g is due to the required symmetry of the associated wave function of the scattering process. The connection between these spin-dependent cross-sections and the 'normal' differential cross-section $\sigma(\theta, E)$ for unpolarized electrons and atoms is given by the relation

$$\sigma(\theta, E) = \tfrac{1}{2}\{|f|^2 + |g|^2 + |f - g|^2\}, \tag{2.1}$$

where $|f - g|^2 = |f|^2 + |g|^2 - 2|f|\,|g|\cos\phi$, and ϕ is the phase difference between f and g. We obtain

$$\begin{aligned}\sigma(\theta, E) &= |f|^2 + |g|^2 - |f|\,|g|\cos\phi \\ &= \sigma_{\rm d} + \sigma_{\rm ex} - \sigma_{\rm int}.\end{aligned} \tag{2.2}$$

The factor $\frac{1}{2}$ in equation (2.1) takes account of the fact that only 50% of the possible reactions are of reactions (1)–(3) in table 1. A simple calculation results in the familiar relations

$$\begin{aligned}\sigma(E, \theta) &= |f|^2 + |g|^2 - {\rm Re}(f^* g) \\ &= \tfrac{3}{4}|f - g|^2 + \tfrac{1}{4}|f + g|^2 \\ &= \tfrac{3}{4}|T|^2 + \tfrac{1}{4}|S|^2 = \tfrac{3}{4}\sigma_T + \tfrac{1}{4}\sigma_S \\ &= \tfrac{1}{2}\sigma^{\uparrow\downarrow} + \tfrac{1}{2}\sigma^{\uparrow\downarrow},\end{aligned} \tag{2.3}$$

where $T = f - g$ and $S = f + g$ are the *triplet* and *singlet scattering amplitudes*, $|T|^2 = \sigma_T$ and $|S|^2 = \sigma_S$ are the triplet and singlet cross-sections, and

$$\sigma^{\uparrow\uparrow} = \sigma_T = |f - g|^2 \quad \text{and} \quad \sigma^{\uparrow\downarrow} = |f|^2 + |g|^2 = \tfrac{1}{2}\sigma_T + \tfrac{1}{2}\sigma_S,$$

are further definitions. The interference term,

$$\sigma_{\rm int} = {\rm Re}(f^* g) = |f|\,|g|\cos\phi,$$

leads to constructive ($\phi = 180°$) or destructive ($\phi = 0°$) interference contributions to the cross-sections. The terms 'triplet' and 'singlet' are standard notations taken from spectroscopic notations of atomic states (e.g. for the helium atom).

In ideal scattering experiments, which have, so far, only been possible and successful in a limited way, the polarization of the electrons and atoms before and after scattering (notations $\boldsymbol{P}'_{\rm e}$ and $\boldsymbol{P}'_{\rm a}$) are required in order to obtain complete information on the amplitudes f and g (figure 1). However, measurement of the polarization $\boldsymbol{P}'_{\rm e}$ and $\boldsymbol{P}'_{\rm a}$ after the collision is very difficult for reasons of intensity. On the other hand, combinations of measurements of the spin reactions in table 2 are now possible.

In the first two reactions, only polarized atoms are required; both the polarizations of the electrons and atoms after scattering and the differential cross-section have to

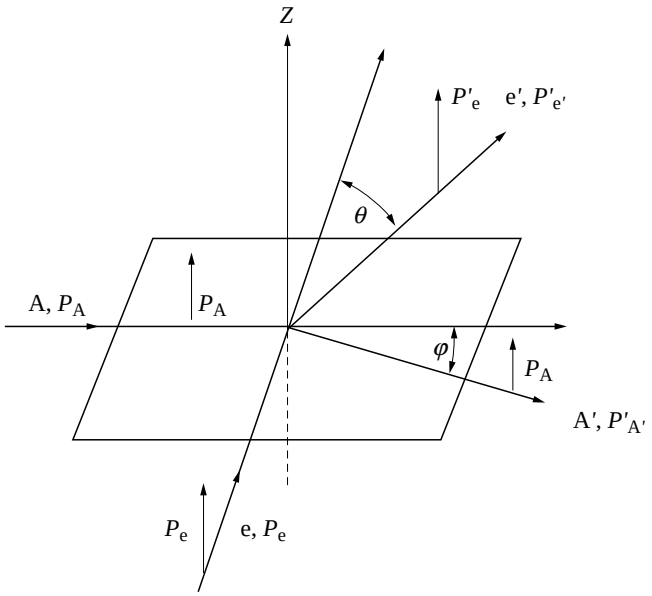

Figure 1. Geometry for scattering polarized electron beams (e, $\boldsymbol{P}_\mathrm{e}$) on polarized atomic beams (A, $\boldsymbol{P}_\mathrm{a}$). $\boldsymbol{P}'_\mathrm{e}$ and $\boldsymbol{P}'_\mathrm{a}$ are vector degrees of polarization after scattering.

Table 2.

polarization before collision	measurable quantities after collision	information on the collisions process
(1) $\boldsymbol{P}_\mathrm{a} \neq 0$, $P_\mathrm{e} = 0$	$\boldsymbol{P}'_\mathrm{e}$, $\sigma(E,\theta)$	$\lvert f\rvert^2 = \sigma(E,\theta)(1 - P'_\mathrm{e}/P_\mathrm{a})$
(2) $\boldsymbol{P}_\mathrm{a} \neq 0$, $P_\mathrm{e} = 0$	$\boldsymbol{P}'_\mathrm{a}$, $\sigma(E,\theta)$	$\lvert g\rvert^2 = \sigma(E,\theta)(1 - P'_\mathrm{a}/P_\mathrm{a})$
(3) $\boldsymbol{P}_\mathrm{a} \neq 0$, $P_\mathrm{e} = 0$	$\sigma(E,\theta)$	$\lvert f-g\rvert^2 = \sigma + (1 + P_\mathrm{e}/P_\mathrm{a})(I - \sigma)$
	$I(E,\theta) = I_\mathrm{e}^{\uparrow} + I_\mathrm{e}^{\downarrow}$	$I(E,\theta) = \sigma(E,\theta) - P_\mathrm{e}P_\mathrm{a}\,\mathrm{Re}(f^*g)$
	$= I_\mathrm{a}^{\uparrow} + I_\mathrm{a}^{\downarrow}$	equivalent to $\cos\phi$ (equation (2.2))

be measured in order to obtain $|f|^2$ and $|g|^2$. In the third reaction, the cross-section $I(E,\theta)$ for the scattering intensity of polarized electrons or of polarized recoil atoms has to be measured in which, in addition, P_e and P_a and the cross-section $\sigma(E,\theta)$ have to be known in order to determine $|f-g|^2$ or the phase term $\cos\phi$.

Another measurable quantity is the *spin asymmetry*, which is linked to the above quantities and can be defined as follows:

$$A = \frac{1}{P_\mathrm{e}P_\mathrm{a}}\frac{\sigma^{\uparrow\downarrow} - \sigma^{\uparrow\uparrow}}{\sigma^{\uparrow\downarrow} + \sigma^{\uparrow\uparrow}} = \frac{\sigma_\mathrm{int}}{\sigma}. \tag{2.4}$$

The same equation is valid for the case in which the differential cross-sections σ, $\sigma^{\uparrow\downarrow}$, $\sigma^{\uparrow\uparrow}$ and σ_int are replaced by the corresponding total cross-sections Q, $Q^{\uparrow\downarrow}$, $Q^{\uparrow\uparrow}$ and Q_int.

The pioneering work for the production of polarized beams of electrons is based on the spin–orbit interaction in the so-called *Mott scattering* of electrons in the pure

Coulomb field of the nucleus. Shull *et al.* (1943) were the first to detect spin-polarized electrons from the scattering of energetic electrons (40 keV) on thin gold foils. However, according to theoretical predictions by Massey & Mohr (1941), electron spin polarization can also occur for low-energy electron scattering (less than or equal to 2 keV). This polarization effect is due to an interference between electrons scattered directly in the atomic field without spin-flip and those scattered with spin-flip (see below for the connection between the amplitude h and k in equation (2.6)). Following a proposal by Kollath (1949), Deichsel (1961) succeeded in detecting electron spin polarization in low-energy scattering of electrons by mercury atoms. An electron-scattering current of 10^{-9} A and an electron spin polarization of 17% was measured for elastic scattering of 300 eV electrons by mercury atoms (Steidl *et al.* 1965). The most successful method for the production of spin-polarized electrons to date is based on photoemission in special solids such as gallium arsenides (GaAs) and gallium arsenide phosphides (GaAsP).

Metallo-organic chemical vapour deposition of GaAs–GaAsP photocathodes ('strained-layer photocathodes') has recently resulted in a production of over 90% spin-polarized electron beams. The current of polarized electron beams can be as high as that of unpolarized beams, and is usually limited by space-charge effects in the electron-beam optics.

Polarized atoms can be produced by the following methods:

(1) by means of spatial separation of atoms into different Zeeman components m with a magnetic hexapole field;

(2) by redistribution of Zeeman components m of the atoms by optical pumping; and

(3) by combinations of both methods (1) and (2).

While Stern–Gerlach and Rabi magnets separate atomic beams in different magnetic substates m from each other, a magnetic hexapole focuses atoms in certain m states and defocuses atoms in other m states. The production of polarized atoms by means of magnets is based on the existence of magnetic moments μ in atoms that experience a magnetic force $\mu\partial B/\partial r$; this force has different signs for the quantum numbers $\pm m$ of the atom. The magnetic-field inhomogeneity $\partial B/\partial r$ varies proportionally to the distance from the centre of a hexapole magnet. The trajectories of atoms of a spin component $m_s = +1/2$ are bent towards the centre of the hexapole magnet, while those with $m_s = -1/2$ are bent away from it. Single-electron atoms in n^2S states without nuclear spins (which unfortunately do not exist in nature) would be expected to be polarized to 100% by the action of a hexapole field. The spins of the focused atoms are orientated parallel to the local $\boldsymbol{B}$ field in the hexapole magnet. When the atoms leave the hexapole magnet, they are expected to orientate themselves adiabatically (i.e. gradually) with the direction of an external magnetic field. This guiding magnetic field has to be very small in realistic scattering experiments in order to keep the influence of the Lorentz force on the electron to a minimum. This minimal magnetic field results in a reduced effective spin polarization, due to the fact that the electron spin is associated with relevant magnetic moments of the hydrogen or alkali atoms. The nuclear spin I and the electron spin S couple to the total spin F, so that the electron spin polarization of the atom is reduced from 100%

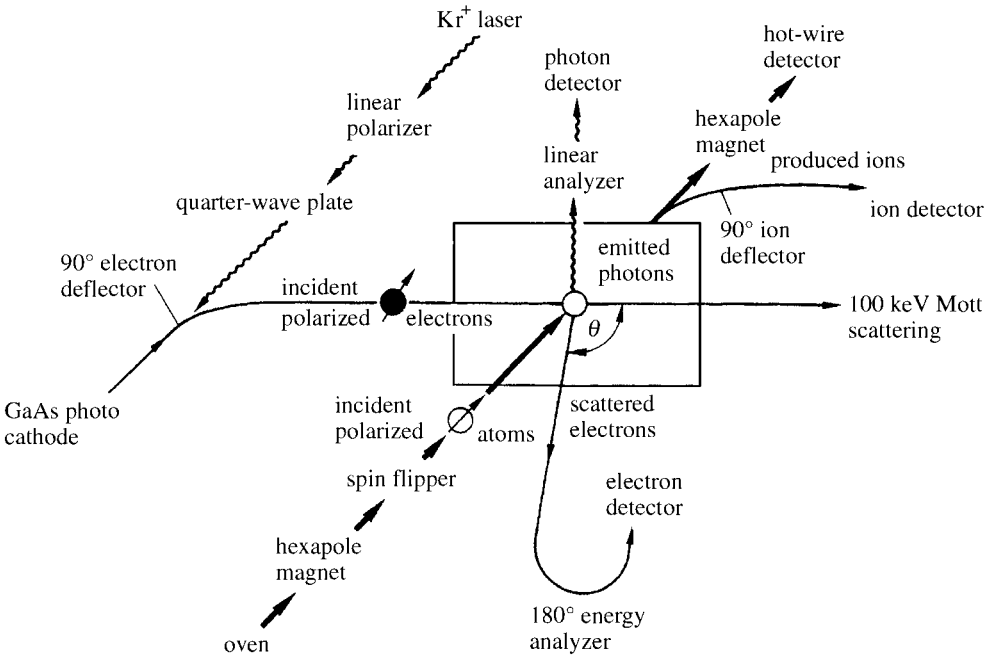

Figure 2. Scheme of a universal apparatus for studying elastic and inelastic scattering and ionization in collisions between polarized electrons and polarized atoms. The photodetector serves for the detection of asymmetries of inelastic excitation processes (after Raith 1988).

to $P_{\mathrm{a}} = 1/(2I+1)$, since further magnetic hyperfine components are associated with electron spin components in the opposite direction, i.e. $m_{\mathrm{s}} = -1/2$. In other words, the maximum electron spin polarization produced by the hexapole field and the guiding magnetic field becomes 50% for atomic hydrogen ($I = 1/2$), 33% for ^{6}Li ($I = 1$), 25% for ^{23}Na ($I = 3/2$) and only 12.5% for caesium ($I = 7/2$). By applying the method of optical pumping with circularly polarized light, substantially larger degrees of polarization can be obtained for the above atoms. Optical pumping with circularly polarized light from the $[F = I + 1/2]$ ground state into the $[F' = F + 1]$ state of the excited $^2\mathrm{P}_{3/2}$ state has the consequence that the largest m_F state of the $[I + 1/2]$ ground state is populated preferentially. The nuclear and electron spins in the magnetic substate ($m_F = I + 1/2$) are then orientated in the same direction. However, the electron spin polarization of the atom is not complete, since the ($m_F = I + 1/2$) ground state is not altered in its m_F population, and, accordingly, its spin components m_{s} remain unpolarized. The resulting electron spin polarizations of the atoms can be calculated as $P_{\mathrm{a}} = (I+1)/(2I+1)$ based upon this method, e.g. to $P_{\mathrm{H}} = 75\%$, $P_{\mathrm{Li6}} = 66.7\%$ and $P_{\mathrm{Na23}} = 62.5\%$.

For a further increase in the spin polarization, the two methods of applying hexapoles and optical pumping have been combined.

With regard to a modern apparatus for scattering of polarized electrons on polarized atoms, we refer to the schematic arrangement in figure 2. The instrumental complexity speaks for itself. Apart from investigating elastic and inelastic scattering processes, the setup for such experimental arrangements can also be used for studying ion asymmetries in electron impact ionizations. The *ion asymmetry* A_{ion} follows,

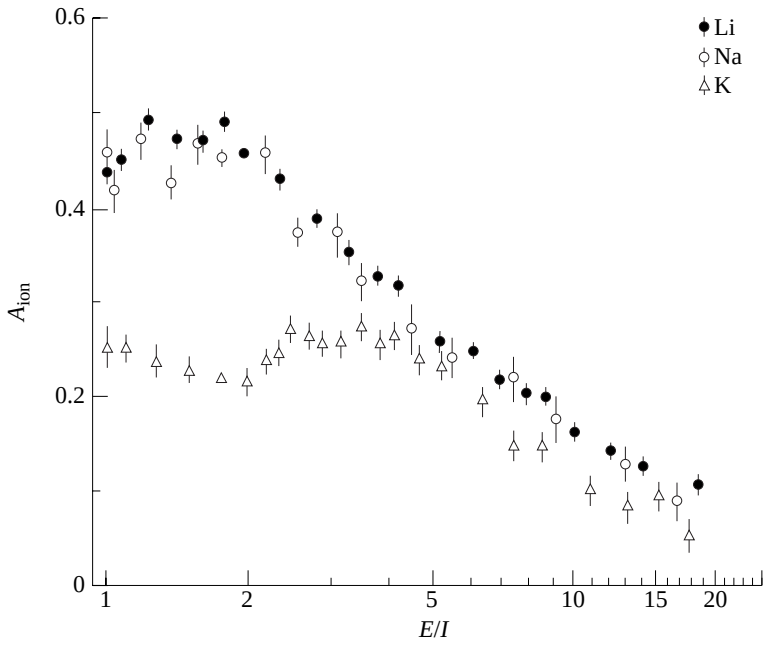

Figure 3. Ion asymmetries $A_{\text{ion}} = [N^{\uparrow\uparrow}(I) - N^{\uparrow\downarrow}(I)/N^{\uparrow\uparrow}(I) + N^{\uparrow\downarrow}(I)]$ from scattering of polarized electrons on polarized light alkali metal atoms. E/I is the ratio of the energy of the incident electrons to the ionization energy of the relevant atom (after Baum *et al*. 1985).

in analogy to equation (2.4), from the difference number $N(I)$ of the ions produced in the ionization process, in which the arrows refer to initially parallel or antiparallel orientated spins of electrons and atoms:

$$A_{\text{ion}} = \frac{N^{\uparrow\uparrow}(I) - N^{\uparrow\downarrow}(I)}{N^{\uparrow\uparrow}(I) + N^{\uparrow\downarrow}(I)}. \tag{2.5}$$

Out of the considerable number of investigations with polarized electrons and polarized atoms, we select, as illustrative examples, measurements of ion asymmetries and the quantity $|f|^2/\sigma$ in table 2 for one-electron atoms (figures 3 and 4). Historically, ion asymmetries were the first spin quantities extracted from experiments with polarized electrons and polarized atoms in the second half of the 1970s. The observation of an astonishingly large ion asymmetry (figure 3), which shows up as an integral effect in the total ionization cross-section, was a surprise in the physics of electron impact ionization.

As an example of spin effects in elastic electron–atom scattering, figure 4 shows a distinctive interference structure in the intensity of the electron scattering by polarized potassium atoms, which manifests itself in the 'direct' Coulomb interaction (amplitude f). The basic experiment for the underlying scattering process consists of the measurement of the polarization of the scattered electrons, which were initially unpolarized (see reaction (1) in table 1).

Passing on to electron scattering by heavy atoms such as rubidium and caesium, spin–orbit interaction between the projectile electron and the target atom takes place in addition to the direct Coulomb and exchange interaction. This situation is similar to the description of the normal fine structure of excited atoms, or the photoionization

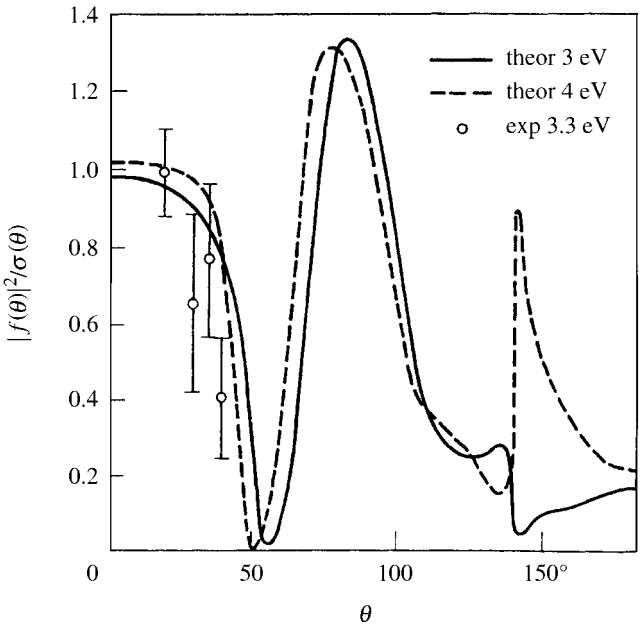

Figure 4. Experimental (○) and theoretical data for the square of the direct elastic scattering amplitude, f, divided by the differential cross-section $\sigma(\theta)$ as a function of the scattering angle, θ, with polarized potassium as target atoms. The experimental data follow from the measurement polarization of initially unpolarized electrons scattered elastically on partially polarized potassium atoms ($P_a = 20\%$). (Reaction (1) from table 1; after Hils *et al.* (1972).)

of heavy alkali atoms where spin–orbit interactions increase with the larger masses of atoms involved. Six amplitudes are necessary for the description of the electron scattering on heavy alkali atoms, which means that 11 independent quantities, i.e. six moduli and five phase differences, have to be determined for a complete analysis of the scattering process (Burke & Mitchell 1974; Khalid & Kleinpoppen 1983).

The complication due to the large number of amplitudes is reduced by using target atoms without a resulting zero electron spin ('spinless atoms'), as, for example, with rare-gas atoms or two-electron atoms. Two spin reactions can be defined for the scattering of polarized electrons on spinless atoms:

(1) $\mathrm{e}(\uparrow) + \mathrm{a} \rightarrow \mathrm{a} + \mathrm{e}(\uparrow)$, h, $|h|^2$;

(2) $\mathrm{e}(\uparrow) + \mathrm{a} \rightarrow \mathrm{a} + \mathrm{e}(\downarrow)$, k, $|k|^2$.

We denote the first process, as before, as a *direct process with amplitude* h and the second one as a *spin-flip process with amplitude* k. We note that the direct process can be superposed coherently with an electron exchange process; the direct process and the exchange process cannot be separated from each other due to their indistinguishability in the experiment. In order to measure the amplitudes h and k, partly polarized electrons are to be scattered by atoms; the change of the spin polarization of the electrons after scattering determines the moduli $|h|$ and $|k|$ and

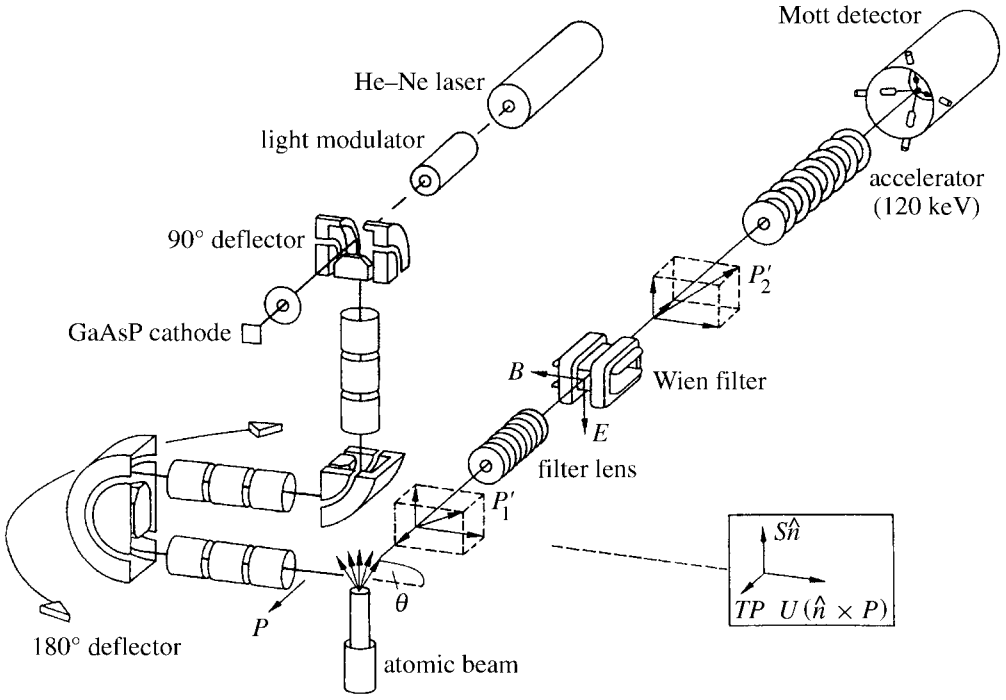

Figure 5. Scheme of an apparatus for scattering partially polarized electrons on spinless atoms (after Berger & Kessler 1986).

their phase difference $\Delta\varphi = \gamma_1 - \gamma_2$ based on the following relations:

$$S = -\frac{2|h||k|\sin\Delta\varphi}{\sigma}, \qquad T = \frac{|h|^2 - |k|^2}{\sigma}, \qquad U = \frac{2|h||k|\cos\Delta\varphi}{\sigma}, \tag{2.6}$$

where $\sigma = |h|^2 + |k|^2$ is the differential cross-section; and the quantities S, T and U are connected to the components of the spin polarization of the scattered electrons as follows

$$P_\mathrm{e} = S\boldsymbol{n} + T\boldsymbol{P}_\mathrm{e} + U(\boldsymbol{n} \times \boldsymbol{P}_\mathrm{e}). \tag{2.7}$$

$\boldsymbol{P}_\mathrm{e}$ is the vector polarization of the scattered electrons under the condition that the initial spin polarization of the incoming electrons is in the scattering plane. The quantity $S\boldsymbol{n}$ is the component of the spin of the scattered electrons perpendicular to the scattering plane (i.e. in the direction of the scattering normal), $T\boldsymbol{P}_\mathrm{e}$ is parallel or antiparallel to $\boldsymbol{P}_\mathrm{e}$, and $U(\boldsymbol{n} \times \boldsymbol{P}_\mathrm{e})$ is rotated by 90° with reference to $\boldsymbol{P}_\mathrm{e}$ in the scattering plane. Figure 5 displays the schematic layout for such experiments. The method of production of polarized electrons and the polarization measurement by the Mott detection has been described above.

The *Wien filter* has two orthogonally superimposed magnetic and electric fields and acts on the electron beam as follows. Electrons of a given fixed energy pass through the Wien filter only if the Lorentz force due to the magnetic field has the right size; in this way the Wien filter acts as an energy or velocity filter. In addition, the spin components $\boldsymbol{P}_\mathrm{e}$ and $S\boldsymbol{n}$, orientated perpendicular to the magnetic field, can carry out Larmor precessions, i.e. these spin components may be rotated by 90°

according to the choice of the magnetic field strength. In this way, it is possible to transform the longitudinal spin component into a transverse one, which is required for the measurement of the polarization by means of the Mott detector. From the measurements of the quantities S, T and U, the relevant amplitudes and their phase differences can be calculated as

$$|h| = [\tfrac{1}{2}\sigma(1+T)]^{1/2},$$
$$|k| = [\tfrac{1}{2}\sigma(1-T)]^{1/2},$$
$$\gamma_1 - \gamma_2 = \tan^{-1}(-S/U),$$

according to equation (2.6). Figure 6 shows an example of these quantities for elastic electron–xenon scattering. As one can see in this figure, the modulus $|h|$ of the direct scattering amplitude shows a distinctive diffraction structure, which is due to the superposition of several partial waves of scattered electrons with various angular momenta. This structure is determined by the dipole and exchange interaction, which can be described in connection with the Ramsauer–Townsend effect. The modulus of the spin-flip amplitude $|k|$, which originates from the spin–orbit interaction, is considerably smaller than that of the direct amplitude $|h|$; the spin-flip amplitude is primarily determined by the $(l = 1)$ partial wave of the scattered electrons, which has the result that the diffraction structure is hardly discernible.

We note that the measurement of the complex amplitudes h and k signifies a *'complete experiment'*. 'Complete' means, for our example, a measurement based on a physical method that allows one to determine the complex amplitudes h and k; however, because of coherent superposition of the Coulomb-direct, Coulomb-exchange and spin–orbit interactions of this collision process, it is not possible to determine the amplitudes of these interactions.

In the research literature in electron–atom collisions, the above amplitude h and k for the direct and spin-flip process are denoted by the letters f and g. Unfortunately, this leads to a confusion with regard to the description of the direct Coulomb interaction (normally associated with the amplitude f) and the Coulomb-exchange interaction (normally associated with the amplitude g) in electron scattering by atomic hydrogen and light alkali atoms (equation (2.1)).

3. Spin parameters extracted from polarized electrons on polarized caesium atoms

Burke & Mitchell (1974) developed a theory that includes, in addition to the Coulomb-direct and Coulomb-exchange effects, spin–orbit interactions. Application to heavy alkalis such as caesium atoms leads to the six complex scattering amplitudes $a_1, a_2, a_3, a_4, a_5, a_6$ (i.e. six moduli and five phase differences). The expected minimum of 11 measurements would determine completely the six complex amplitudes; however, this number of 11 is increased to 18 measurements due to complex independence of some of the scattering amplitudes (Khalid & Kleinpoppen 1983). To transform the collision matrix of Burke & Mitchell (1974) into a form that enables us to see the connections to the previous triplet (T) and singlet (S) amplitudes (or Coulomb-direct (f) and exchange amplitudes (g), i.e. $\{\frac{1}{2}(S+T) = f, \frac{1}{2}(S-T) = g\}$),

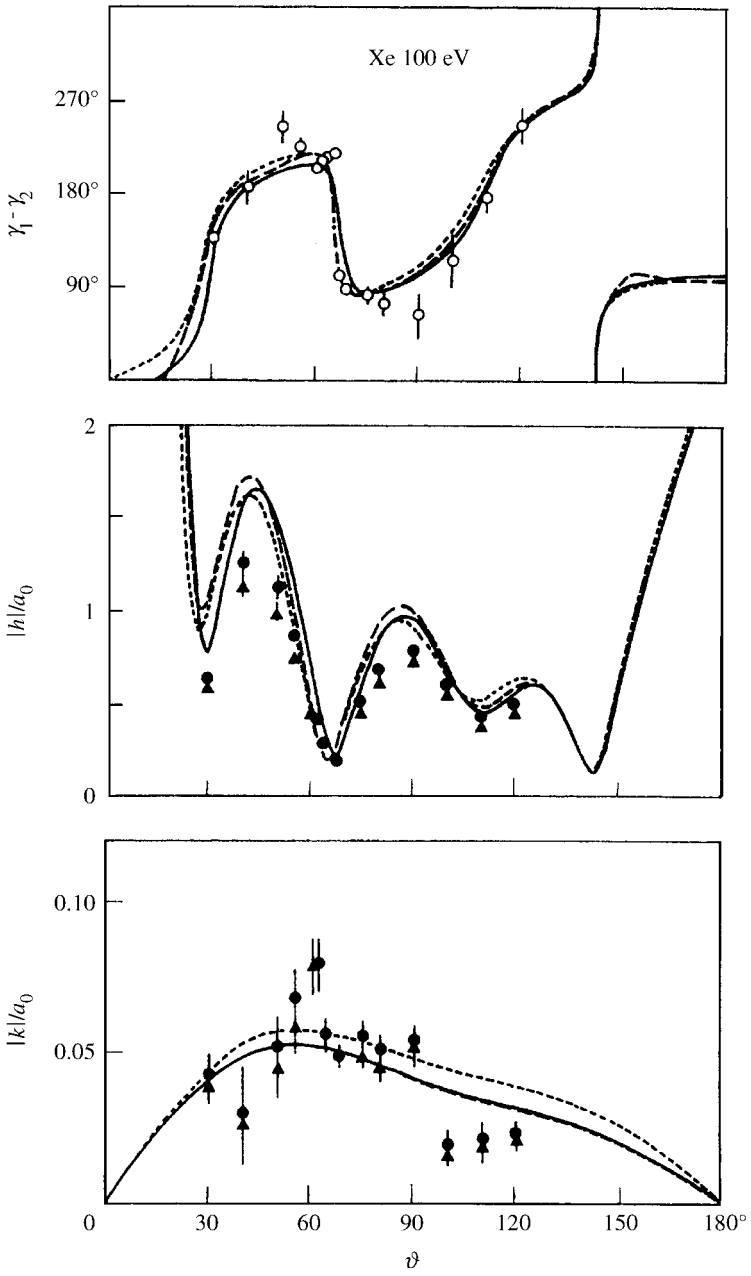

Figure 6. Moduli of amplitudes $|h|$ and $|k|$ and phase differences $\gamma_1 - \gamma_2$ between the two amplitudes for elastic scattering of polarized electrons on xenon atoms, as a function of the scattering angle at an energy of 100 eV. Experimental data points with error bars are after Berger & Kessler (1986). The dotted and full curves represent various theoretical predictions: (——) after Haberland *et al.* (1986); (· · · · ·) after McEachran & Stauffer (1986); and (– – –) after Awe *et al.* (1983). The data for $|h|$ and $|k|$ are given in units of the Bohr radius a_0, and are normalized to the measured differential cross-section $\sigma = |h|^2 + |k|^2$.

we obtain a set of the following amplitudes:

$$\left.\begin{aligned} f_1 &= a_1 + a_5 \cos^2 \tfrac{1}{2}\theta + a_6 \sin^2 \tfrac{1}{2}\theta, \\ f_2 &= (a_1 + a_4) - (a_5 - a_6)\cos\theta, \\ g &= a_1 - a_4 - a_5 - a_6, \\ h_1 &= -(1/\sqrt{2})[(a_5 - a_6)\sin\theta + \mathrm{i}(a_2 + a_3)], \\ h_2 &= (1/\sqrt{2})[(a_5 - a_6)\sin\theta = \mathrm{i}(a_2 + a_3)], \\ k &= (\mathrm{i}/\sqrt{2})(a_2 - a_3), \\ m &= -a_4 + a_5 \sin^2 \tfrac{1}{2}\theta + a_6 \cos^2 \tfrac{1}{2}\theta, \end{aligned}\right\} \tag{3.1}$$

where θ is a scattering angle. When there is no spin–orbit interaction, we use eqn (12) of Burke & Mitchell (1974), with $f_1 = f_2$, as the triplet amplitude, and g as the singlet amplitude, i.e.

$$h_1 = h_2 = k = m = 0,$$

and by inspection of (2.6) we get

$$a_2 = a_3 = 0, \qquad a_4 = a_5 = a_6,$$

which is eqn (2) of Farago (1974).

By applying the general scattering geometry as shown in figures 1 and 2, the differential cross-section σ with both partial spin polarizations of the incoming electron beam ($\hat{\boldsymbol{P}}_\mathrm{e}$ as polarization unit vector of the electron), and the atoms ($\hat{\boldsymbol{P}}_\mathrm{a}$ as polarization unit vector of the atoms) perpendicular to the scattering plane, can be expressed based upon the theory of Burke & Mitchell (1974) as follows:

$$\sigma = \sigma_0[1 + A_1(\hat{\boldsymbol{P}}_\mathrm{a} \cdot \hat{\boldsymbol{n}}) - A_{nn}(\hat{\boldsymbol{P}}_\mathrm{e} \cdot \hat{\boldsymbol{n}})(\hat{\boldsymbol{P}}_\mathrm{a} \cdot \hat{\boldsymbol{n}})].$$

The unit vector $\hat{\boldsymbol{n}}$ is orthogonal to the scattering plane and points in the direction of the atomic beam.

The collision matrix can be constructed with the components of the spin perpendicular to the scattering plane, and can express the asymmetries introduced above by the six independent amplitudes a_i ($i = 1$–6):

$$\left.\begin{aligned} A_1 &= 2\,\mathrm{Re}(a_1 a_2^* + a_3 a_4^*)/\sigma_0, \\ A_2 &= 2\,\mathrm{Re}(a_1 a_3^* + a_2 a_4^*)/\sigma_0, \\ A_{nn} &= 2\,\mathrm{Re}(-a_1 a_4^* - a_2 a_3^* + a_5 a_6^*)/\sigma_0, \end{aligned}\right\} \tag{3.2}$$

with the cross-section of unpolarized particles given by

$$\sigma_0 = \sum_{i=1}^{6} |a_i|^2.$$

The amplitudes $(a_1 + a_2 + a_3 + a_4)$ and $(a_1 - a_2 - a_3 + a_4)$ describe scattering where spins both before and after the collision are aligned parallel and antiparallel to the normal of the scattering plane, respectively. The amplitudes $(-a_5 + a_6)$ describe scattering where the change in the spin components normal to the scattering plane satisfies $\Delta M_S = \pm 2$ and $\Delta M_S = 0$, respectively, with reorientation of the individual components ($\Delta m_i \neq 0$). The amplitude $(a_2 - a_3)$ is connected with spin non-conserving collisions, that is transitions from $S = 1, 0$ to $S = 0$, $M_S = 0$ states. The amplitude a_3 is the 'standard' spin–orbit amplitude, i.e. responsible for the spin

dependence of Mott scattering. The amplitude a_2 can be interpreted as describing the influence of *spin-other-orbit* collision effects (between the valence-electron spin and scattered-electron orbit). In the absence of spin–orbit interaction, the amplitudes acquire the following values, expressed through the customary triplet (t) and singlet (s) or direct (f) and exchange (g) scattering amplitudes:

$$a_1 = (\tfrac{3}{4})t + (\tfrac{1}{4})t + (\tfrac{1}{4})s = f - (\tfrac{1}{2})g,$$
$$a_4 = a_5 = a_6 = (\tfrac{1}{4})t - (\tfrac{1}{4})s = (\tfrac{1}{2})g, \qquad a_2 = a_3 = 0.$$

The equation for A_1 contains an interference term $a_3 a_4^*$ between the spin–orbit (a_3) and exchange-related (a_4) processes; the term $a_1 a_2^*$ is zero when the spin–orbit interaction is negligible. It follows that A_1 is only non-zero if spin–orbit and exchange effects are simultaneously present in the scattering process.

The asymmetry A_2, is mainly determined by the combination $(a_1 a_3^*)$, the spin–orbit amplitude a_3 in connection with the scattering amplitude a_1. Consequently, while A_2 appears as a 'direct spin–orbit asymmetry' (without exchange interaction), A_1 might be called '*exchange spin–orbit asymmetry*'. If the amplitude a_2 is negligible, the asymmetry A_{nn} vanishes in the absence of exchange interactions; therefore, it can be named *'exchange asymmetry'*.

In the experiment by Baum *et al.* (1997), the polarized electron beam is produced by photoemission of a strained GaAs crystal (polarization $P_\mathrm{e} = 65\%$, electron current 0.5 μA, energy spread $\Delta E = 150$ meV). The spin-polarized caesium beam is produced by laser optical pumping, with two laser diodes in single mode operation tuned to transitions from the hfs ground states with $F = 4$ and $F = 3$ to the $6^2\mathrm{P}_{3/2}$ excited states with $F' = 5$ and $F' = 4$, respectively. The light is made circularly polarized with a linear polarizer and a quarter-wave plate. They obtain nearly perfect polarization with a value of $P_\mathrm{a} = 0.9$ at an atomic beam density of $\rho = 5 \times 10^9$ cm^{-3} in the scattering centre. Continuous operation of the atomic beam is possible for over 200 h, after which time the recirculating oven is depleted of *caesium*. Measured relative to each other are the four spin-dependent differential cross-sections expressed in the following equations:

$$\sigma^{\uparrow\uparrow} = \sigma_0(1 + A_1 P_\mathrm{a} + A_2 P_\mathrm{e} - A_{nn} P_4 P_\mathrm{e}),$$
$$\sigma^{\downarrow\uparrow} = \sigma_0(1 - A_1 P_\mathrm{a} + A_2 P_\mathrm{e} + A_{nn} P_2 + P_\mathrm{e}),$$
$$\sigma^{\uparrow\downarrow} = \sigma_0(1 + A_1 P_\mathrm{a} - A_2 P_\mathrm{e} + A_{nn} P_\mathrm{a} P_\mathrm{e}),$$
$$\sigma^{\downarrow\downarrow} = \sigma_0(1 - A_1 P_\mathrm{a} - A_2 P_\mathrm{e} - A_{nn} P_\mathrm{a} P_\mathrm{e}).$$

These asymmetries for the spin asymmetries A_1 and A_2 are normalized to the product $P_\mathrm{a} P_\mathrm{e}$.

Measurements of differential cross-sections on caesium were critically tested in the intermediate energy range (20, 13.5, 7 eV). For the first time, a distinctly non-zero asymmetry in A_1 was observed whose measurement was first proposed by Farago (1974, 1976). Figures 7–10 show the most recent results at 3 eV for the electron–caesium elastic scattering. The cross-section data (figure 7) are in good agreement with other experimental and theoretical results, except with regard to the Dirac theory, which has the minimum near the forward direction at smaller scattering angles and not as deep as in other theories.

The experimental spin asymmetry data A_{nn} (figure 8) for the angular interval from $\theta = 60°$ to 125° agree reasonably well with certain theoretical predictions,

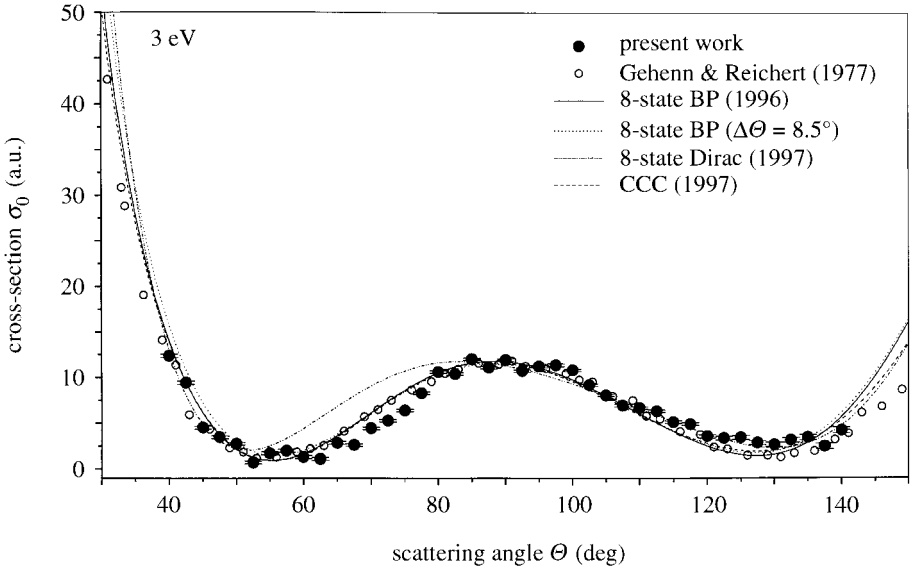

Figure 7. Cross-section (relative) measured at 3 eV in comparison with the experimental work of Gehenn & Reichert (1977) and with theoretical results (Bartschat & Bray 1996; Bartschat 1993, personal communication; Ait-Tahar *et al*. 1997; Bray, personal communication) as indicated. For the eight-state Breit–Pauli data, the results of convolution theory with the experimental angular resolution are shown as an example. The normalization was performed at 90°.

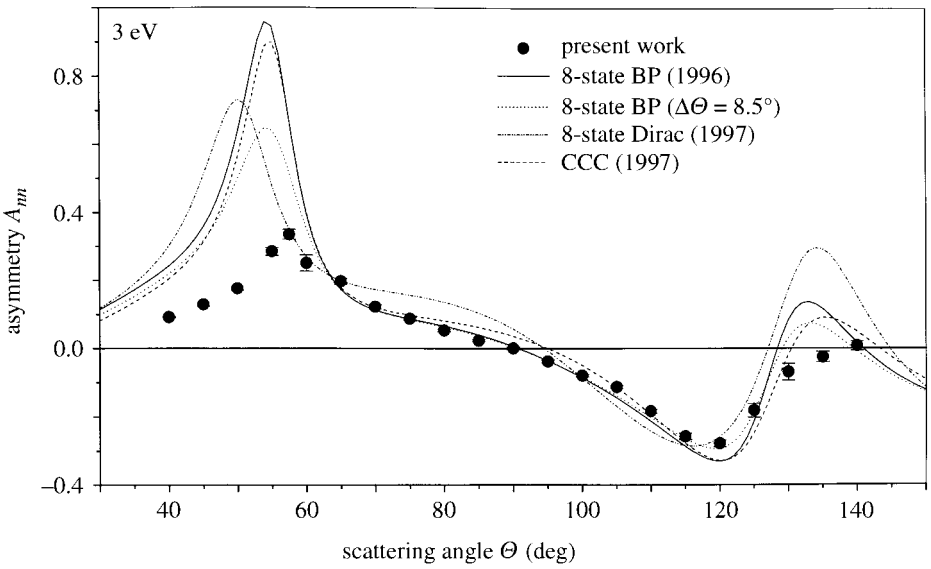

Figure 8. Spin asymmetry A_{nn} ('exchange') measured at 3 eV in comparison with theoretical results (Bartschat & Bray 1996; Bartschat, personal communication; Ait-Tahar *et al*. 1997; Bray, personal communication) as indicated. Only statistical errors are shown on the data points. For the eight-state Breit–Pauli data, the effect of convoluting theory with experimental angular resolution is shown as an example.

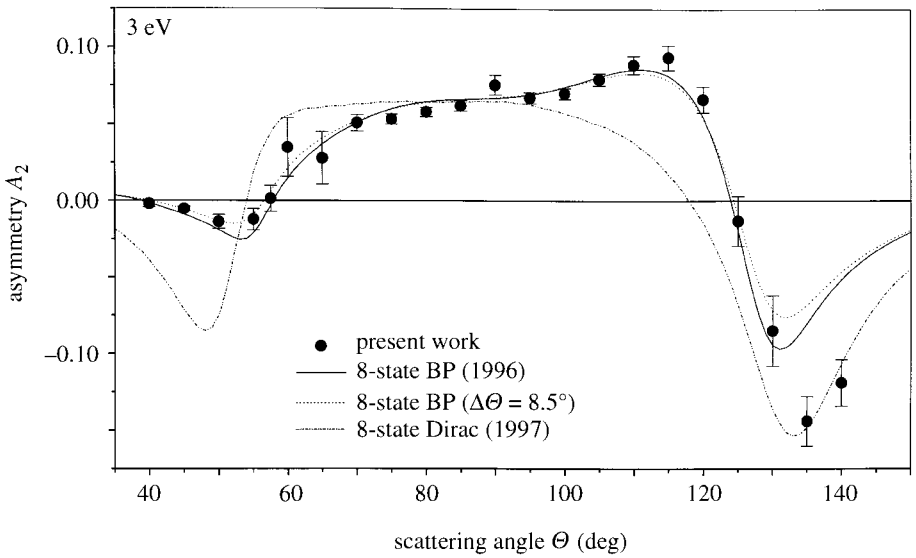

Figure 9. Spin asymmetry A_2 ('direct spin orbit') measured at 3 eV in comparison with theoretical results (Bartschat, personal communication; Ait-Tahar *et al.* 1997) as indicated. Only statistical errors are shown on the data points. For the eight-state Breit–Pauli data, the effect of convoluting theory to the experimental angular resolution is shown as an example.

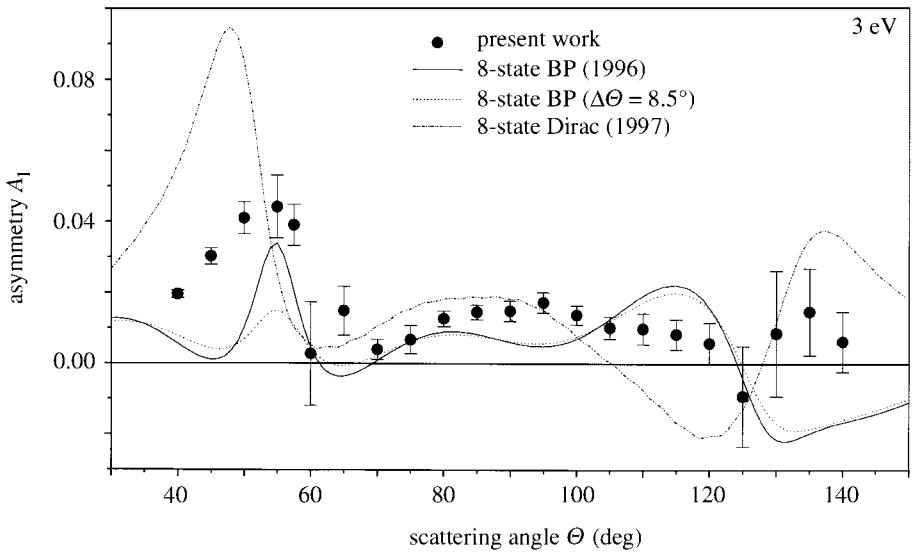

Figure 10. Spin asymmetry A_1 ('exchange spin orbit') measured at 3 eV in comparison with theoretical results (Bartschat, personal communication; Ait-Tahar *et al.* 1997) as indicated. Otherwise as figure 7.

with the Dirac results showing the largest deviations for comparison. However, near $\theta - 55°$ and $\theta - 130°$ (cross-section minima), the theories predict some pronounced structure that is not well reflected by the experimental data, but reveals a tendency to diminishing asymmetries.

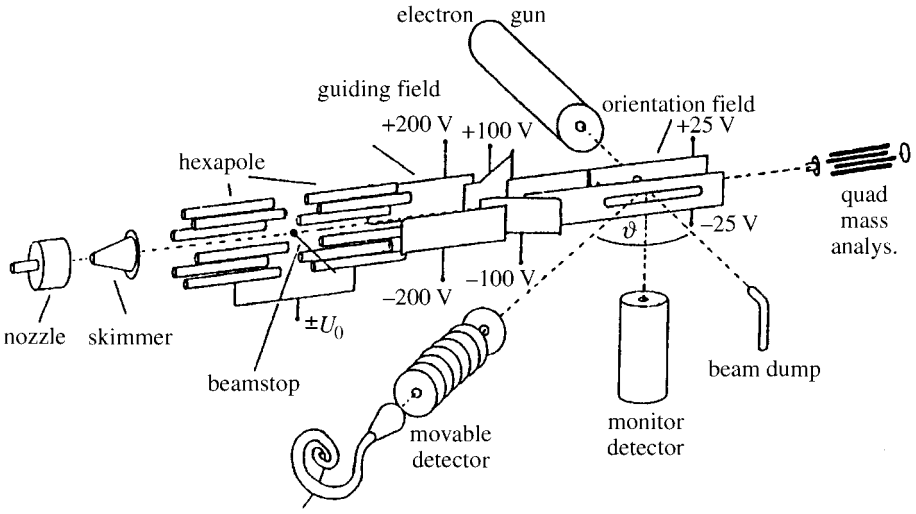

Figure 11. Experimental apparatus for elastic electron scattering from hexapole state selected and orientated molecules (Böwering 1998).

The experimental A_2 data in figure 9 show nearly perfect agreement with the two Breit–Pauli approximations, only the two measured data points at the largest backward scattering angles are significantly lower than the predictions of these theories. The theoretical predictions (preliminary) of the Dirac treatment deviate considerably from the Breit–Pauli theory and are also in disagreement with the experimental data, particularly in the angular interval from 30° to 50° and from 11° to 130°.

The spin asymmetry A_1 (figure 10) contains exchange and relativistic effects. The two Breit–Pauli approximations display distinctly different results, showing a sharp asymmetry peak near the forward direction; however, in the forward and backward directions, these approximations display considerably different sizes, locations and even opposing angular variation and signs. The measurements agree reasonably well with theories in the angular range from 60° to 105°.

By comparing theoretical and experimental data from all three asymmetries, it is somewhat surprising that the experiment does not show the sharp structure in A_{nn} near the forward scattering that is predicted by the theories. Possible minute contaminations in the caesium beam would reduce the measured asymmetry. However, it is certainly surprising that the measured asymmetry A_1 is large compared to the Breit–Pauli approximations near the forward direction. Further important studies to exclude any influence from contaminations are underway, since the statistical error of the asymmetries in the angular range from 40° to 140° is only $\delta A < 0.005$ for e–Cs scattering at 3 eV.

4. Electron scattering interactions with orientated molecules

While many atomic and molecular collision applications have already been carried out with orientated molecules, in this section, we will restrict ourselves to electron scattering by orientated molecules, which results in additional molecular structure information and alignment properties of the sample molecules. We report, here, on experimental data obtained by the research group of Böwering (1998), who applied

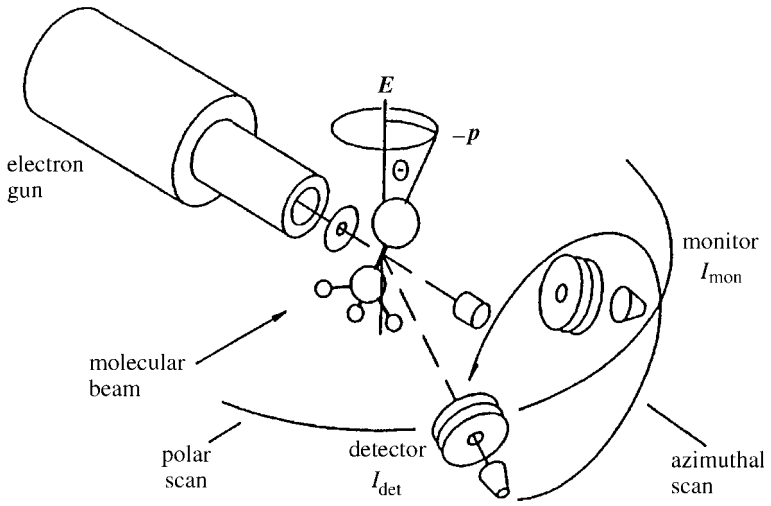

Figure 12. Scheme of the electron beam unit for scattering experiments of electrons by orientated molecules indicating polar and azimuthal detection geometries (Böwering 1997).

the electrostatic hexapole technique to orientate molecules. Molecules that give rise to a linear Stark effect can be orientated in electric fields after state selection in a strong electrostatic hexapole field (figure 11). Depending on the hexapole voltage U_0, different states are focused through a guiding field into the scattering region and are orientated with preferential direction of their internuclear axis in a weak homogeneous electric orientation field. For a continuous molecular beam with a relatively high rotational temperature T_{rot}, many rotational states are usually present in the focus region, and their contributions have to be weighted accordingly. By combining such a molecular beam apparatus with an electron-scattering unit, the first measurements of differential cross-sections for orientated molecules were obtained in 1992 (Volkmer *et al*. 1992). A continuous supersonic jet of CH_3I or CH_3Cl molecules, for example, is generated with rotational temperatures of approximately either 70 or 25 K by a nozzle-skimmer arrangement. After passage through the electrostatic hexapole and the guiding electric field, the molecules are orientated preferentially parallel or antiparallel to the electron beam.

With the orientation field directed either parallel or antiparallel to the electron beam, scattering occurs when either the methyl group or the halogen atom of the CH_3I or the CH_3Cl molecules is pointing preferentially towards the incident electrons. Figure 12 illustrates the detection scheme used for perpendicular orientation direction of the molecules to the electron beam direction (typically 1 keV electron energy, 10 μA electron current). The elastic electron-scattering distribution is recorded by a rotatable detector consisting of a retarding field-energy analyser and channeltron detector. It was found that by switching the guiding field on and off, the molecular orientation could be turned on and off without influencing the electron beam. In this way, the additional molecular-interference term $\bar{M}(\vartheta, \chi)$ for the focused state ensemble can be determined as a fraction of the differential cross-section $\sigma_{\mathrm{unor}} = (\mathrm{d}\sigma/\mathrm{d}\Omega)_{\mathrm{unor}}$ from measurements of the scattering intensity for orientated, I_{or}, and

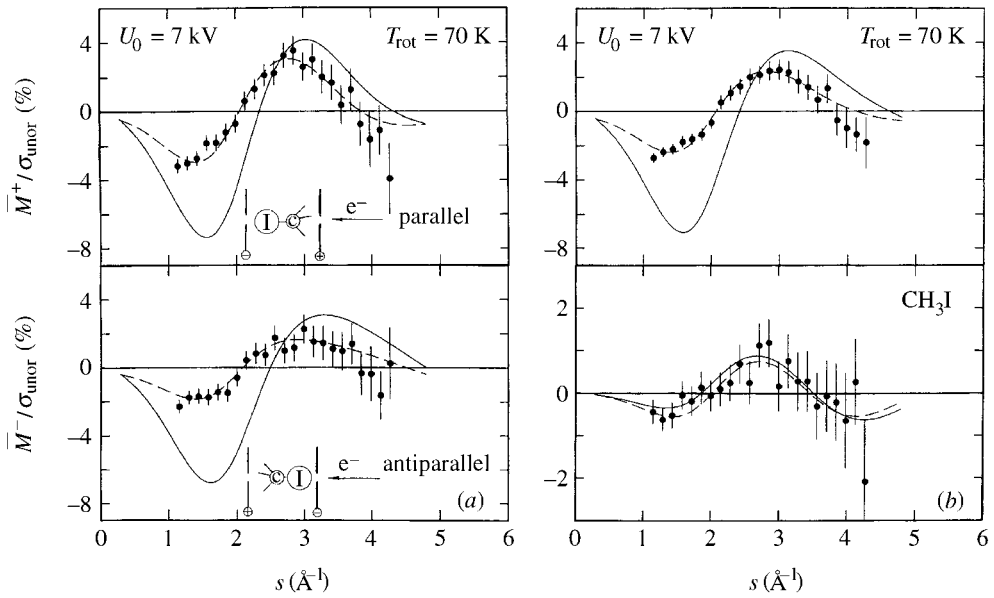

Figure 13. Measured normalized molecular orientational interference contributions for CH_3I (Volkmer *et al.* 1996) as a function of momentum transfer, obtained at $U_0 = 7$ kV and at 1 keV scattering energy: results for parallel and antiparallel orientation, as well as pure alignment and orientation parts. IAM model calculations (——); Legendre polynomial fit (– – –).

for unorientated molecules, I_{unor}, according to

$$\frac{\bar{M}(\vartheta,\chi)}{\sigma_{unor}(\vartheta)} = \frac{I_{or}(\vartheta,\chi) - I_{unor}(\vartheta,\chi)}{I_{unor}(\vartheta,\chi)}.$$

The molecular orientational interference terms $\bar{M}^+$ and $\bar{M}^-$ for the parallel/antiparallel scattering geometry (molecular orientation parallel or antiparallel to the electron beam direction) can be divided into even and odd parts (representing pure alignment and pure orientation contributions):

$$\bar{M}^{\pm} = \bar{M}_a(s) \pm \bar{M}_0(s).$$

In a first series of experiments on CH_3I (Volkmer *et al.* 1992, 1996) and CH_3Cl (Böwering *et al.* 1994), a cylindrically symmetric scattering geometry was chosen with the orientation field directed either parallel or antiparallel to the electron beam so that the scattering occurs when either the methyl group or the halogen atom is pointing preferentially towards the incident electrons. Figures 13 and 14 show typical results for the mean interference terms for orientated CH_3I and CH_3Cl molecules obtained for a molecular state ensemble focused at a hexapole voltage of $U_0 = 7$ kV and under expansion conditions such that T_{rot} is *ca.* 70 K. For the momentum transfer studied (corresponding to a range of polar angles ϑ from 4° to 15°), a distinct oscillatory pattern is observed with deviations from the scattering from orientated molecules of several per cent. The full curves indicate model calculations that were also carried out by applying the 'independent atom model' (IAM) of Kohl & Shipsey (1992), to the state ensemble determined by hexapole transmission calculations. They

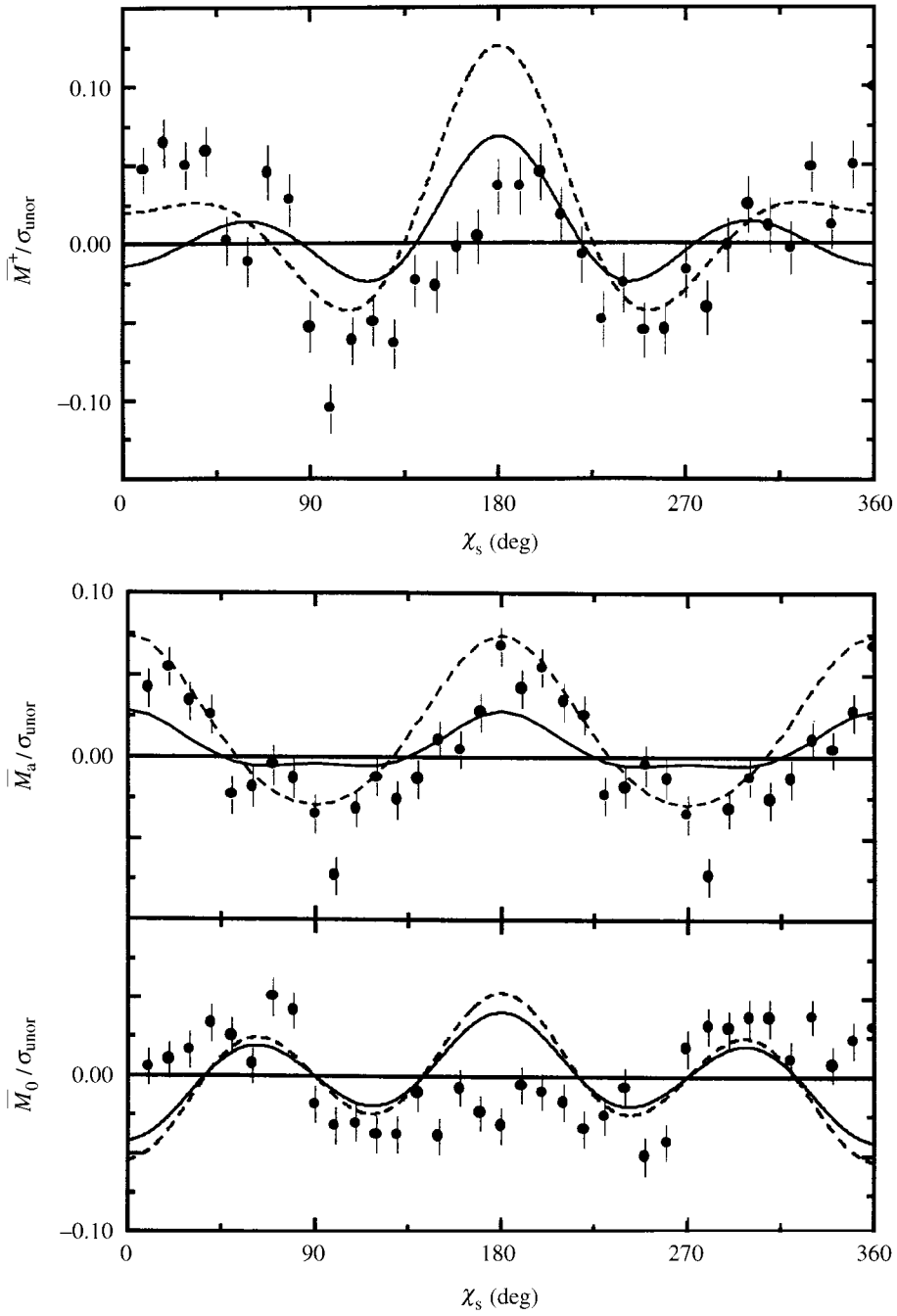

Figure 14. Measured azimuthal distribution of the normalized molecular orientational interference term for perpendicular orientation of CH_3Cl molecules at a fixed polar angle of 8° and $U_0 = 4$ kV. IAM calculations using only the linear Stark effect (– – –) or the linear and quadratic Stark effect (——) are shown for comparison (Volkmer *et al.* 1997).

show good agreement for the pure orientation contributions, but deviate at small values of the momentum transfer s in the alignment part. In order to demonstrate the analysis of molecular orientational anisotropies, a fit of the experimental distributions was carried out (dashed lines in figure 13) and the leading Legendre moments characterizing the orientation of the state ensemble were extracted. Scattering distributions were obtained for 700 eV, 1000 eV and 1250 eV electron energy; the results indicated a significant dependence of the orientational interference terms on the scattering energy.

In experiments with CH_3Cl (figure 14), similar results were obtained at comparable conditions, except that the pure orientation contributions were very small. By a variation of the hexapole voltage, the effective mean degree of orientation can be changed. The use of different expansion conditions, with higher or lower stagnation pressures and different nozzle diameters, leads to a change in the rotational temperatures of the molecules. When the degree of orientation or the rotational temperature are changed, pronounced alterations of the resulting scattering patterns are observed, reflecting the high sensitivity of the method of the spatial distribution of the molecular axis orientations. A comparison with model calculations indicated that the observed changes were mainly due to the changed population fractions of the $|111\rangle$ and $|222\rangle$ states (Böwering *et al*. 1994).

For *steric* information, the axial collision symmetry has to be removed and the azimuthal dependence of the cross-section has to be recorded as well (case illustrated in figure 12). Azimuthal distributions were measured for CH_3Cl (figure 14) molecules orientated preferentially perpendicular to the incident electrons by using electric field plates rotated by 90° and by scanning a detector at a fixed polar angle on a full circle around the electron beam direction (see figure 12). As shown in figure 14, pronounced orientation-dependent angular variations are found in both experiment and corresponding IAM calculations at a fixed angle of $\vartheta = 8°$. The measured scattering distribution can be divided into even and odd parts, $\bar{M}_a$ and $\bar{M}_0$, respectively. For comparison with the data, IAM calculations have been carried out for this perpendicular geometry. Refined model calculations, which also take into account the quadratic Stark effect when calculating the state ensemble produced by the hexapole focusing (see also Ohoyama *et al*. 1995), lead to a significant change, and give better agreement with the experimental data. The modelling of the azimuthal and polar electron-scattering distributions has revealed the importance of the accuracy of the calculated state populations, and has not, so far, given any indication that the IAM description is not sufficiently precise for this application.

The results of Böwering's group have clearly demonstrated that molecular-interference terms in the electron scattering by molecules may occur which are very sensitive to the spatial distribution of the orientation of the molecular axis.

5. Spin and polarization effects in photoionization of atoms

Single- and multielectron effects determine the photoionization of atoms in general. Spin and spin–orbit interaction effects in the photoionization of atoms can in particular be studied by photoelectron spin experiments and by applying polarized atoms in the photoionization process. The former type of experiment has been particularly successful when used in photoionization of rare-gas atoms and adsorbates, and reviews on the results are available (see, for example, Heinzmann 1992), while the

latter type of experiment and related theories have in particular been applied in recent years to photoionization of atoms with partly filled sub-shells. The British physicist M. J. Seaton and the American physicist J. W. Cooper showed that the finite value in the minimum of the cross-section of heavy alkali metal atoms (e.g. rubidium or caesium) is due to a spin–orbit interaction W_{LS}; it has its origin in the fine-structure interaction between the magnetic moment $\boldsymbol{\mu}$ of the photoelectron and the motional magnetic field, $\boldsymbol{B}$, that the electron experiences in the Coulomb field of the ion produced, i.e. $W_{LS} = -(\boldsymbol{\mu} \cdot \boldsymbol{B})$. In other words, this description incorporates the same interaction that we use in the analysis of the spectroscopic fine structure. However, in the case of the photoionization, the photoelectron is in an unbounded continuum state.

An interesting photoelectron spin-effect is associated with this spin–orbit interaction, which was first predicted by Fano (and is, therefore, called the *Fano effect* (Fano 1969*a*, *b*)). Although both continuum states $\varepsilon\,^2\mathrm{P}_{1/2,3/2}$ of the photoelectrons are degenerate in their energies, the radial parts $R(\varepsilon, j = 3/2) = R_3$ and $R(\varepsilon, j = 1/2) = R_1$ of the relevant matrix element for the photoionization are different from each other, due to the spin–orbit interaction; i.e. since $R_3 \neq R_1$, their cross-sections are different, and the spin–orbit interaction causes the continuum wave function with $j = 1/2$ to be attracted to the ion by a small amount, while the continuum wave function with $j = 3/2$ is pushed away from the ion by a small amount.

Experimental data for the spin polarization of photoelectrons of caesium as a function of the wavelength of the incoming circularly polarized photons have been reported extensively (see, for example, Heinzmann *et al*. 1970); these data convincingly demonstrate the existence of the *Fano effect*. The maximum of *ca*. 100% spin polarization lies within the area of the minimum of the photoionization cross-section as expected from theoretical arguments.

A complementary method for investigating the Fano effect and the amplitudes and phases of photoionization has been applied by using spin-polarized atoms as targets. For example, Baum *et al*. (1972) carried out photoionization experiments with polarized Cs, Rb and K atoms in their ground states (electron spin $s = 1/2$); they measured the numbers, $N^{\uparrow}$ and $N^{\downarrow}$, of the ions produced in which the spins of atoms were either parallel ($\uparrow$) or antiparallel ($\downarrow$) to a given quantization direction. The asymmetry $A = (N^{\uparrow} - N^{\downarrow})/(N^{\uparrow} + N^{\downarrow})$ is related, theoretically, to the spin polarization of the photoelectrons of the Fano effect as discussed above, i.e. the ratio R_3/R_1 can be related to the asymmetry A and, hence, it can be determined. Historically, these asymmetry experiments were the first ones to detect the Fano effect.

As an extension of photoionization experiments with spin-polarized atoms, it has been shown theoretically (Klar & Kleinpoppen 1982) that the measurement of angular distributions of photoelectrons, originating from polarized atoms, allows one to determine not only ratios of the matrix elements but also their phase differences. Without discussing theoretical details, we give some examples of the photoionization of excited atoms. A beam of metastable neon atoms in the Ne ($2\mathrm{p}^5 3\mathrm{s}, {}^3\mathrm{P}_{0,2}$) states, which can be produced in a DC discharge tube (density approximately equal to 10^6–10^7 cm^{-3}), is crossed by photons of a dye ring laser, which induce transitions from the metastable $^3\mathrm{P}_2$ state into the Ne ($2\mathrm{p}^5 3\mathrm{p}, {}^3\mathrm{D}_3$) state. It is important that the intensity of the laser radiation is sufficient to produce an unequal population of the magnetic substates m_j of the $^3\mathrm{D}_3$ state by means of optical pumping between the $^3\mathrm{P}_2$ and $^3\mathrm{D}_3$ states with linearly or circularly polarized light, i.e. an alignment of unequal

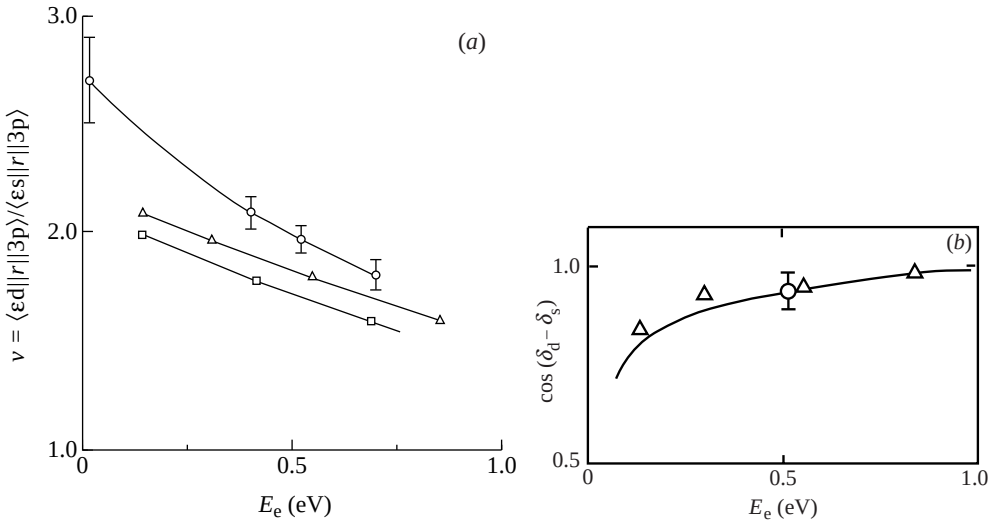

Figure 15. Experimental data (○) (after Siegel *et al*. 1983): (*a*) for $\nu = \langle \epsilon d|\,|r|\,|3p\rangle/\langle \epsilon s|\,|r|\,|3p\rangle$; and (*b*) for $\cos(\delta_d - \delta_s)$ of the photoionization of the Ne $(2p^5 3p,\ ^3D_3)$ state as a function of the energy of photoelectrons compared to theoretical results: (△) many-body of perturbation multi-configuration close coupling theory (after Chang 1982); (□) multi-configuration close configuration calculation (after Luke 1982); the full line in part (*b*) follows from quantum-defect theory calculated by Siegel *et al*. (1983).

population of the $|m_j|$ states by optical pumping with linearly polarized light or an orientation with an unequal population of the m_j states by optical pumping with circularly polarized light. The photoionization from the Ne $(2p^5 3p, {}^3D_3)$ state can be described by the two matrix elements $\langle \epsilon d|\,|r|\,|3p\rangle$ and $\langle \epsilon s|\,|r|\,|3p\rangle$ with the transitions into the orbital continuum states ϵs and ϵd; the phases δ_d and δ_s of the matrix elements correspond to the phases of outgoing s and d waves of the photoelectron. Figure 15 shows results of the ratio $\nu = \langle \epsilon d|\,|r|\,|3p\rangle/\langle \epsilon s\|r\|3p\rangle$ and of $\cos(\delta_d - \delta_s)$ as a function of the energy of the photoelectrons. These quantities are very sensitive tests for theoretical models of photoionization. Photoionization of aligned and excited $(6s6p)\,{}^3P_1$ ytterbium atoms by laser radiation were also investigated, and resulted in ratios of matrix elements and their relevant phase differences (Kerling *et al*. 1990). In addition, we refer to further publications on 'complete' analysis of photoelectrons in the region of autoionizing states (Kabachnik & Sazhina 1976, 1990; Hausmann *et al*. 1988; Ueda *et al*. 1993; Becker 1990).

Photoionization angular distributions of the $2s^2$ and $2p^4$ subshells of atomic oxygen (Plotzke *et al*. 1996) have been studied at various angular positions of the photoelectrons, for which figures 16 and 17 show, schematically, the experiment and results of a distinct linear magnetic dichroism in the angular distribution of the $2p^4$ subshell ionization of atomic oxygen in the process

$$\mathrm{O}\ (1s^2 2s^2 2p^4)\,{}^3P_2 + h\nu \rightarrow \mathrm{O}^+\ (1s^2 2s^2 2p^3)\,{}^4S_{3/2} + e^-.$$

The important conclusion from these data is that, in addition to the cross-section σ and the traditional angular parameter β, a further parameter β' is required to

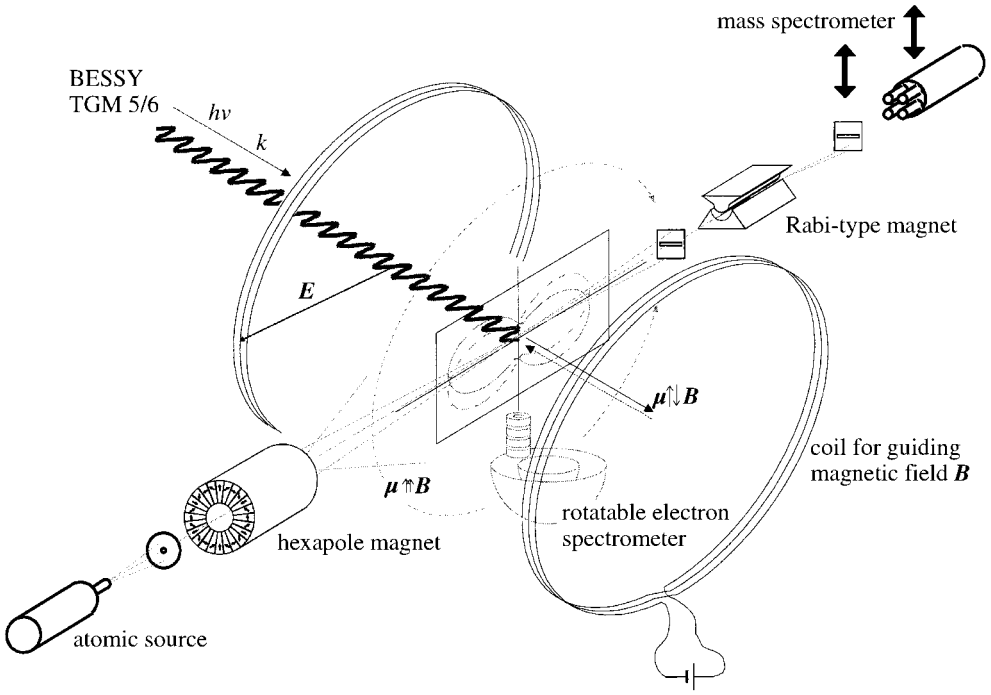

Figure 16. Schematic of the experiment including the atomic source, a collimator, the hexapole magnet, the rotable electron spectrometer, a Rabi magnet, mass spectrometer, the incoming synchrotron radiation from BESSY TGM6, and the magnetic coil pair for the guiding field (after Plotzke *et al*. 1996).

describe the observed angular distribution of figure 17:

$$I_{\pm}(\theta) = C_I \frac{\mathrm{d}\sigma_{\pm}}{\mathrm{d}\omega}(\theta)$$
$$= C_I \frac{\sigma}{4\pi}[c_1(1 + \tfrac{1}{4}\beta[1 + 3P_1\cos(2\theta)) \pm c_2\beta' P_1 \sin(2\theta)].$$

The factor C_I accounts for the target density, the reaction volume, the detection efficiency, the light intensity, etc. The factors c_1 and c_2 depend on the M_J population numbers.

The guiding magnetic fields $\boldsymbol{B}$ for the polarization direction of the atoms were parallel $\boldsymbol{B} \uparrow\uparrow \boldsymbol{k}$ or antiparallel to $\boldsymbol{B} \uparrow\downarrow \boldsymbol{k}$ of the incoming light. The degree of linear polarization $P_1 = 0.99 \pm 0.01$ of the synchrotron radiation was determined by analysing the He 1s photoelectron angular distribution.

The positive sign of the last term refers to the case $\boldsymbol{B} \uparrow\uparrow \boldsymbol{k}$, the negative one to $\boldsymbol{B} \uparrow\downarrow \boldsymbol{k}$. It was possible to measure β and β' in the photon energy range from *ca.* 25 to 52 eV.

The sum of both count rates $I_+(\theta)$ and $I_-(\theta)$, gives the common β distribution for unpolarized targets.

The count rate difference is

$$I_+(\theta) - I_-(\theta) = 2C_I(\sigma/4\pi)c_2\beta' P_1 \sin(2\theta),$$

which determines the β' parameter with the knowledge of $C_I\sigma$ and P_1. Alternatively, β' can be calculated from the dichroism measured at the quasi-magical angle θ_{mag}

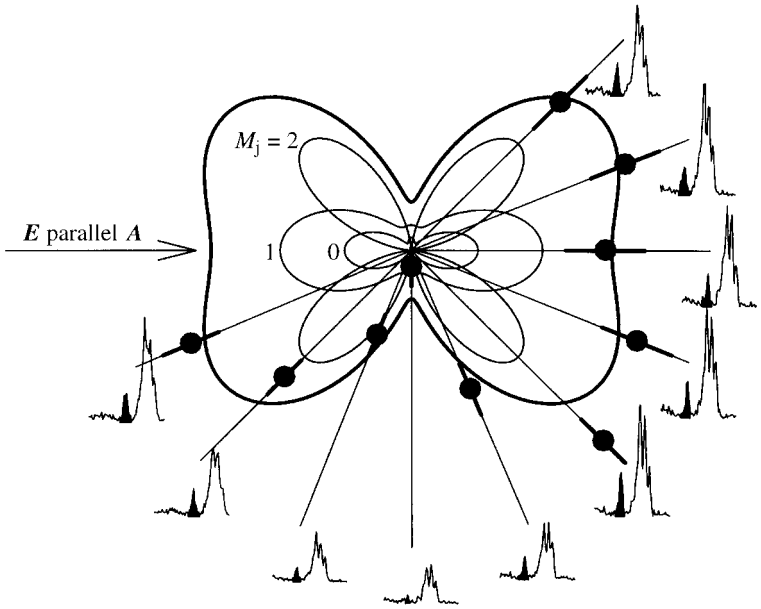

Figure 17. Angular distribution of photoelectrons for polarized atoms. It contains contributions that are not described by $1 + \beta P_2(\cos\theta)$. The filled black peaks in the photoelectron spectra belong to the oxygen atoms, the other peaks next to them are vibrational multiplets of unpolarized molecular oxygen (after Plotzke *et al*. 1996).

without using $C_I\sigma$ or β:

$$\frac{I_+(\theta_{\rm mag}) - I_-(\theta_{\rm mag})}{I_+(\theta_{\rm mag}) + I_-(\theta_{\rm mag})} = \frac{c_2}{c_I} P_1 \beta' \sin(2\theta_{\rm mag}),$$

with

$$\theta_{\rm mag} = \tfrac{1}{2}\cos^{-1}(+1/(3P_1)).$$

In order to interpret the data for the photoelectrons of the reaction O $(2p^4)\,{}^3P_2 + h\nu \rightarrow O^+$ $(2p^3)\,{}^4S_{3/2} + e^-$, we describe the angular distribution of this open shell atom in LS coupling. Neglecting relativistic effects, the measurement of the parameters β and β' can be used to determine the ratio $\gamma = R_{\rm d}/R_{\rm s}$ of the two radial components of the matrix elements for the 2p electron photoionized into εs and εd continuum states, and the difference of asymptotic phase shifts $\Delta = \Delta_{\rm d} - \Delta_{\rm s}$ of these states. The following equations for transformation between (β, β') and (γ, Δ) can be used:

$$\beta_{\rm O\,2p\,{}^4S_{3/2}} = \frac{\gamma[2\gamma + 4\cos(\Delta)}{1 + 2\gamma^2},$$

$$\beta'_{\rm O\,2p\,{}^4S_{3/2}} = -\frac{9\gamma\sin(\Delta)}{2(1 + 2\gamma^2)}.$$

Similar equations hold for the final ionic states ^{2}D and ^{2}P. Possible contributions from the excited fine-structure states $^3P_1$ and $^3P_0$ (gas temperature 300 K) were not resolved. They affect the factors c_1 and c_2 only weakly, so the determination of γ and Δ is possible without knowing the exact population numbers of the fine-structure

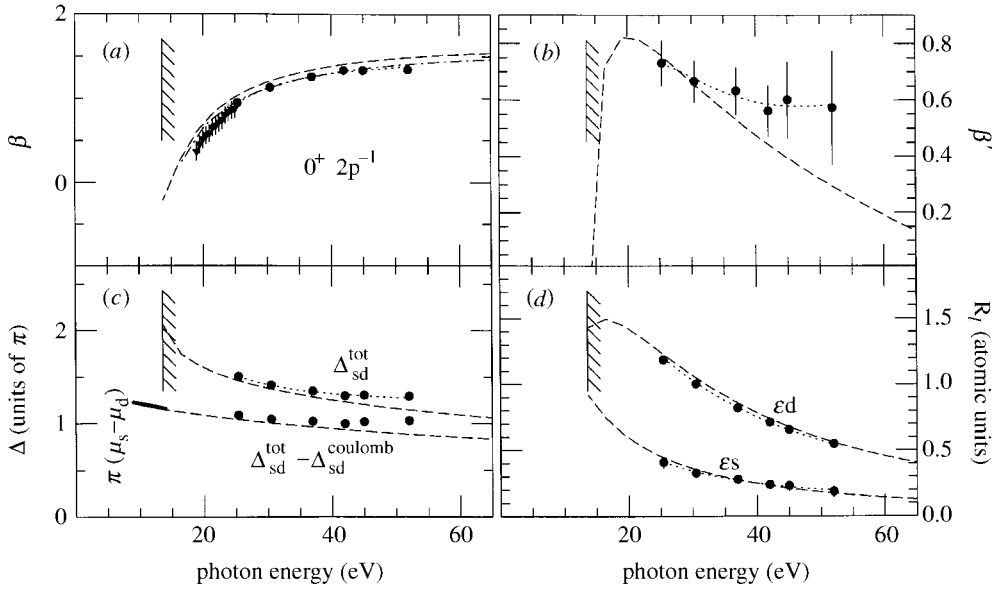

Figure 18. Angular distribution parameters β (a) and β' (b), the difference Δ in the asymptotic phase shift (c), and the partial wave amplitudes (d). The dotted curves are the theoretical result using the Cowan code (Cowan 1981), the dash–dotted curves represent theoretical results from Starace *et al*. (1974) and the β values below 25 eV are from van der Meulen *et al*. (1991). The solid line represents the quantum defect difference of the two ns and nd Rydberg series, which converge to the ^{4}S threshold.

multiplet. The results of the transformation $(\beta, \beta') \rightarrow (\gamma, \Delta)$ are shown in figure 18, along with theoretical calculations using the Cowan code. The transformation to absolute amplitudes by σ (in units of a_0^2), $h\nu$ (in units of rydbergs) and R_s and R_d (in atomic units) was made using an exponential fit through the absolute $2p^4S$ cross-section data from Schaphorst *et al*. (1995) involving a systematic error of 10%. As β and β' are independent quantities, it is not possible to calculate one from the other. However, the result of the transformation $(\beta, \beta') \rightarrow (\gamma, \Delta)$ is not unique, as, generally, the curves of constant β and β' meet in two points. Even though the number of independent measurements equals the number of free parameters, one bit of information is still missing. Far from threshold, the d amplitude is expected to exceed the s amplitude, and, accordingly, one of the solutions can be ignored. In this case, the large error bar of β' only affects the error bar of γ. While the ratio of the radial dipole integrals is almost constant for $h\nu$ from 25 to 52 eV, the total difference in the asymptotic phase shifts Δ changes more than about 30° in this regime; this is mainly due to the difference in Coulomb phase shifts for the two different angular momenta. If the Coulomb phase shift between the d and s waves is subtracted from Δ, the intrinsic phase shift agrees well with the extrapolation of the quantum defect function below the ionization threshold. Theoretical studies did not report the phase difference for the $^4S_{3/2}$ state; however, their β results are in overall good agreement with our experimental and theoretical data.

The magnetic dichroism in the photoelectron spectrum of polarized oxygen atoms

$$\mathrm{O}\ (1s^2 2s^2 2p^4)\,{}^3P_2 + h\nu \rightarrow \mathrm{O}^+\ (1s^2 2s^2 2p^3)\,{}^{2s+1}L_J + e^-,$$

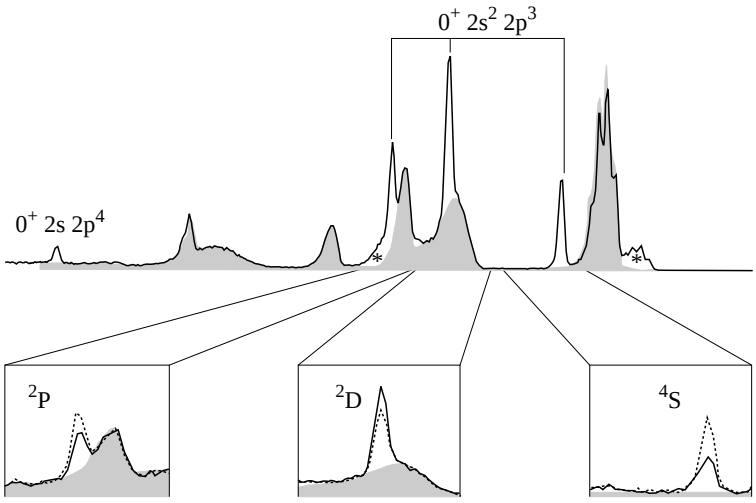

Figure 19. Linear magnetic dichroism of the 2p multiplet in oxygen. The upper part of the figure shows the photoelectron spectrum measured with an effusive unpolarized oxygen at the exit of the RF source. The grey part is the pure O_2 spectrum, with the discharge turned off. The regions marked with $*$ contain distributions from the excited oxygen molecules. The three 2p peaks ^{2}P, ^{2}D and ^{4}S have been obtained using a beam of polarized oxygen atoms with two different polarization directions: II (solid) and III (dashed). The detector position was $\theta = -55°$. In this case, the background contains no contributions from excited molecules.

has also been measured (Prümper *et al*. 1997). In the non-relativistic LS-coupling approximation, the process of photoionizing 2p electrons is completely described by the magnitudes of the s and d partial wave dipole amplitudes, and their phase difference. These three quantities have been determined for atomic oxygen in an angle-resolved photoelectron spectroscopy experiment on polarized atoms. In this parametric representation, the total asymptotic phase shift between the d and the s waves is given by

$$\Delta = \Delta_{\text{Coulombic}} + \Delta_{\text{intrinsic}},$$
$$\Delta_{\text{Coulombic}} = -\pi + \sigma_{l=2} - \sigma_{l=0},$$
$$\sigma_l = \arg\left(\Gamma\left(l + 1 - \mathrm{i}\frac{\hbar}{2\mu E_{\text{kin}} \cdot a_0}\right)\right),$$
$$\Delta_{\text{intrinsic}} = 3.124 - 0.4666\exp[-E_{\text{kin}}/13.95\ \text{eV}] \pm 0.087,$$

where μ is the reduced mass of the electron and a_0 the Bohr radius. Figure 19 displays the linear magnetic dichroism of the 2p multiplet of atomic oxygen. The upper part of the figure shows the photoelectron spectrum measured with an effusive unpolarized oxygen beam at the exit of the radiofrequency source. The grey part is the pure O_2 spectrum with the discharge turned off. The regions marked with $*$ contain contributions from the excited oxygen molecules. The three 2p peaks, ^{2}P, ^{2}D and ^{4}S, were measured using a beam of polarized oxygen atoms with two different polarization directions: II (solid) and III (dashed). The detector position was $\theta = -57°$.

The Coulomb parts are described by the exact solutions for the three Coulomb waves. The parametrization of $\Delta_{\text{intrinsic}}$, as given by the above equation, is a fit

through the experimental data points of Plotzke *et al*. (1996). The original number of three free parameters in the above equation is reduced to one parameter by imposing two boundary conditions, the value of $\Delta_{\mathrm{intrinsic}}$ and its slope $\mathrm{d}\Delta_{\mathrm{intrinsic}}/\mathrm{d}E_{\mathrm{kin}}$ at threshold. The data for these quantities were taken from the numerical result of the Cowan code. An indication of the quality of these results is the good agreement with the quantum defects below threshold. The numerical values 3.142 and 13.95 eV in the above equations are only coincidentally close to π and the binding energy. The ratio of the radial parts of the dipole integrals was found to be almost constant for $E_{\mathrm{kin}} = 10$–50 eV,

$$\gamma = (R_{\mathrm{d}}/R_{\mathrm{s}}) = 2.73 \pm 0.17.$$

Because the absolute value of the radial matrix elements determines the size of the total cross-section only, Δ and γ are sufficient to describe the electron angular distributions, the dichroism and the spin polarization of the photoelectrons. For the sake of completeness only, the third quantity, the total ^{4}S cross-section, is also parametrized using the experimental data of Schaphorst *et al*. (1995):

$$\sigma_{4_S}(E_{\mathrm{kin}}) = 4.79\ \mathrm{Mb} \cdot \exp[-E_{\mathrm{kin}}/32.00\ \mathrm{eV}] \pm 10\%, \quad \text{with Mb as the megabarn unit.}$$

The transformation to atomic units is obtained by the relation

$$\sigma = \tfrac{4}{9}\pi^2 \alpha h\nu \tfrac{4}{9}(R_{\mathrm{s}}^2 + 2R_{\mathrm{d}}^2)$$

(σ in units of a_0^2, $h\nu$ in rydbergs and R_{s} and R_{d} in atomic units).

6. Concluding remarks

As mentioned in the introductory remarks in § 1, the content of this paper is selective in highlighting some of the outstanding recent achievements in atomic and molecular collision physics and photoionization processes of atoms. The concept of *'complete scattering experiments'* in atomic and molecular physics has already been applied in many examples, to the extent that their data output represents the most sensitive tests on theoretical approximations.

Only limited cases show acceptable agreement between theory and experiment, as, for example, in the case of electron impact scattering on simple atoms (see, for example, Anderson *et al*. 1988; Crowe 1997) and (e, 2e) experiments involving polarized electrons (Hanne 1996) or photoionization of basic atoms (see, for example, Becker & Shirley 1996). An interesting paper on photoionization of polarized excited Ar (4p,$J = 3$) atoms near the threshold has been reported by Schohl *et al*. (1997). On the other hand, only very recently, photoionization of heavy atoms with partly filled and polarized subshells led to analyses of 'complete experiments' even with spin or orientation, correlations from outer to inner electron subshells of the atoms (Prümper *et al*. 1999; von dem Borne *et al*. 1998). Electron–fluorescent-photon coincidence spectroscopy of two-electron atoms has been particularly successful in completely analysing photoionization in resonance processes (Beyer *et al*. 1995).

While Burke's outstanding and pioneering papers are spread over various subfields of atomic collision physics, the most relevant one with reference to this article is that of Burke & Mitchell (1974). As the late Sir Harrie Massey mentioned in connection to one of his last lectures presented with the title 'Fundamental processes in atomic collision physics' (see, for example, Lutz *et al*. 1983; Bates 1985), the description of atomic collision processes may be compared to analysing atomic

states in spectroscopy, i.e. by means of gross, fine and hyperfine structures. However, while atomic spectroscopy dominantly requires a *static* theoretical analysis, atomic collision physics needs a *dynamical* analysis and interpretation. Burke and his many collaborators and visitors have followed Massey's and Bates's vision, and created a world centre of atomic and molecular collision physics in Belfast. We feel most honoured to dedicate this article to Phil Burke.

We thank our colleagues N. Cherepkov, B. Langer, O. Plotzke, G. Prümper and B. Zimmermann for valuable discussions and advice in preparing this selective review. H.K. is grateful to the European Union (Brussels) and the Leverhulme Trust (London) for support.

References

Ait-Tahar, S., Grant I. P. & Norrington, P. H. 1997 *Phys. Rev.* **54**, 3984.

Anderson, N., Gallagher, J. W. & Hertel, I. V. 1988 *Phys. Rep.* **165**, 1.

Awe, B., Kemper, F., Rosicky, F. & Feder, R. 1983 *J. Phys.* B **16**, 603.

Bartschat, K. 1993 *J. Phys.* B **26**, 3695.

Bartschat, K. & Bray, I. 1996 *Phys. Rev.* A **54**, 1723.

Bates, D. R. 1985 In *Fundamental processes of atomic collision physics*, p. 1. New York: Plenum.

Baum, G., Lubell, M. S. & Raith, W. 1972 *Phys. Rev.* A **5**, 1073.

Baum, G., Moede, M., Raith, W. & Schröder, W. 1985 *J. Phys.* B **18**, 531.

Baum, G., Raith, W. & Steidl, H. 1997 Sonderforschungsbereich, SFB 216, University of Bielefeld, Münster, p. 7.

Becker, U. 1990 In *Synchtron radiation experiments on atoms and molecules in the physics of electronic and atomic collisions* (ed. A. Dalgarno, R. S. Freund, P. M. Koch, M. S. Lubell & T. B. Lucartorto), p. 162. AIP Conference Proceedings, no. 205.

Becker, U. & Shirley, D. A. (eds) 1996 *VUV and soft X-ray photoionization*. New York: Plenum.

Berger, O. & Kessler, J. 1986 *J. Phys.* B **19**, 3539.

Beyer, H.-J., West, J. B., Ueda, K. J., Kabachnik, N. M., Hamdy, H. & Kleinpoppen, H. 1995 *J. Phys. Lett.* B **28**, 47.

Böwering, N. 1998 In *The physics of electronic and atomic collisions* (ed. H. P. Winter & F. Aumayr), pp. 259–268. Singapore: World Scientific.

Böwering, M., Volkmer, M., Meier, Ch., Lieschke, J. & Fink, M. 1994 *Z. Phys.* D **30**, 117.

Burke, P. G. & Mitchell, J. F. B. 1974 *J. Phys.* B **7**, 214.

Chang, T. N. 1982 *J. Phys. Lett.* B **15**, 81–85.

Cowan, R. D. 1981 *The theory of atomic structure and spectra*. Los Angeles, CA: University of California Press.

Crowe, A. 1997 In *Photon and electron collisions with atoms and molecules* (ed. P. G. Burke & C. J. Joschain), p. 21. New York: Plenum.

Deichsel, H. 1961 *Z. Phys.* **164**, 156.

Fano, U. 1969*a* *Phys. Rev.* **178**, 131

Fano, U. 1969*b* *Phys. Rev.* **184**, 250.

Farago, P. S. 1974 *J. Phys. Lett.* B **7**, 28.

Farago, P. S. 1976 In *Electron and photon interaction with atoms* (ed. H. Kleinpoppen & M. R. C. McDowell), p. 235. New York: Plenum.

Gehenn, W. & Reichert, E. 1977 *J. Phys.* B **10**, 3105.

Haberland, R., Fritsche, L. & Noffke, J. 1986 *Phys. Rev.* A **33**, 2305.

Hanne, G. F. 1996 In *Selected topics on electron physics* (ed. D. M. Murray Campbell & H. Kleinpoppen), p. 57. New York: Plenum.

Hausmann, A., Kämmerling, B., Kossmann, H. & Schmidt, V. 1988 *Phys. Rev. Lett.* **61**, 2669.

Heinzmann, U. 1992 In *Correlations and polarization in electronic collisions and atomic collisions and* $(e, 2e)$ *reactions* (ed. P. J. O. Teubner & E. Weigold), p. 237. Institute of Physics Conference Series, no. 122. Bristol: IOP.

Heinzmann, U., Kessler, J. & Lorenz, J. 1970 *Z. Phys.* **240**, 42.

Hils, D., McCusker, V., Kleinpoppen, H. & Smith, S. J. 1972 *Phys. Rev. Lett.* **29**, 398.

Kabachnik, N. M. & Sazhina, I. P. 1976 *J. Phys.* B **9**, 1681.

Kabachnik, N. M. & Sazhina, I. P. 1990 *J. Phys. Lett.* B **23**, 353.

Kerling, C., Böwering, N. & Heinzmann, U. 1990 *J. Phys. Lett.* B **23**, 629.

Khalid, S. M. & Kleinpoppen, H. 1983 *Phys. Rev.* A **27**, 236.

Klar, H. & Kleinpoppen, H. 1982 *J. Phys.* B **15**, 933.

Kleinpoppen, H. 1971 *Phys. Rev.* A **3**, 2015.

Kollath, R. 1949 *Physikalische Blätter, Fünfter Jahrgang*, 66.

Kohl, D. A. & Shipsey, E. J. 1992 *Z. Phys.* D **24**, 33.

Luke, T. M. 1982 *J. Phys.* B **15**, 1217.

Lutz, H. O., Briggs, J. S. & Kleinpoppen, H. (eds) 1983 *Fundamental processes in atomic collisions*. New York: Plenum.

McEachran, R. P. & Stauffer, A. D. 1986 *J. Phys.* B **19**, 3523.

Massey, H. S. W. & Mohr, C. B. O. 1941 *Proc. R. Soc. Lond.* A **177**, 341.

Ohoyama, H., Ogawa, K. T. & Kasai, T. 1995 *J. Phys. Chem.* **99**, 13 606.

Plotzke, O., Prümper, G., Zimmermann, B., Becker, U. & Kleinpoppen, H. 1996 *Phys. Rev. Lett.* **77**, 2642.

Prümper, G., Zimmermann, B., Plotzke, O., Becker, U. & Kleinpoppen, H. 1997 *Europhys. Lett.* **38**, 19.

Prümper, G., Zimmermann, B., Langer, B., Becker, U., Cherepkov, N. A. & Kleinpoppen, H. 1999. (In preparation.)

Raith, W. 1988 *Fundamental processes of atomic dynamics* (ed. J. S. Briggs, H. Kleinpoppen & H. O. Lutz), p. 229. New York: Plenum.

Schaphorst, S. L., Krause, M. O., Caldwell, C. D., Saha, H. P., Pahler, M. & Jimenez-Mier, J. 1995 *Phys. Rev.* A **52**, 4657.

Schohl, S., Klar, D., Cherepkov, N. A., Petrov, D., Ueda, K., Baier, S., Kau, R. & Hotop, H. 1997 *J. Phys.* B **30**, 609.

Shull, C. G., Chese, C. T. & Myers, F. E. 1943 *Phys. Rev.* **63**, 29.

Siegel, A., Ganz, J., Bussert, W. & Hotop, H. 1983 *J. Phys.* B **16**, 2945.

Starace, A. F., Manson, S. T. & Kennedy, D. J. 1974 *Phys. Rev.* A **9**, 2453.

Steidl, H., Reichert, E. & Deischel, H. 1965 *Phys. Lett.* **17**, 31.

Ueda, K., West, J. B., Ross, K. J., Beyer, H. J., Hamdy, H. & Kleinpoppen, H. 1993 *J. Phys. Lett.* B **26**, 347.

van der Meulen, P., Krause, M. O. & de Lange, C. A. 1991 *Phys. Rev.* A **43**, 5997.

Volkmer, M., Meier, Ch., Mihill, A., Fink, M. & Böwering, N. 1992 *Phys. Rev. Lett.* **68**, 2289.

Volkmer, M., Meier, Ch., Lieschke, J., Mihill, A., Fink, M. & Böwewring, N. 1996 *Phys. Rev.* A **53**, 1457.

Volkmer, M., Meier, Ch., Lieschke, J., Dreier, R., Fink, M. & Böwewring, N. 1997 *Phys. Rev.* A **56**, R1690.

von dem Borne, A., Dohrmann, Th., Verweyen, A., Sonntag, B., Godehusen, K., Zimmermann, P. & Kabachnik, N. M. 1998 *J. Phys. Lett.* B **31**, 41.

PHILOSOPHICAL TRANSACTIONS OF THE ROYAL SOCIETY A MATHEMATICAL, PHYSICAL & ENGINEERING SCIENCES